Université de Montréal

Calculs de modèles d'atmosphères hors-ETL avec métaux pour les étoiles de type sdO : le cas particulier de SDSS J1600+0748

par

Marilyn Latour

Département de physique

Faculté des arts et des sciences

Mémoire présenté à la Faculté des études supérieures

en vue de l'obtention du grade de

Maître ès sciences (M.Sc.)

en physique

Octobre, 2010

Université de Montréal

Faculté des études supérieures

Ce mémoire intitulé:

Calculs de modèles d'atmosphères hors-ETL avec métaux pour les étoiles de type sdO : le cas particulier de SDSS J1600+0748

présenté par:

Marilyn Latour

a été évalué par un jury composé des personnes suivantes:

Pierre Bergeron,	président-rapporteur
Gilles Fontaine,	directeur de recherche
Pierre Brassard,	membre du jury

Mémoire accepté le: _____

Sommaire

Nous présentons nos grilles de modèles d'atmosphères pour les étoiles sous-naines chaudes de type O (sdO) soit : des modèles classiques hors-ETL H, He, des modèles hors-ETL avec, en plus, du C, N, O et finalement des modèles incluant C, N, O, Fe. En utilisant les raies de Balmer et d'hélium dans le domaine du visible, nous avons fait des comparaisons entre les spectres théoriques de nos différentes grilles afin de caractériser les effets des métaux. On trouve que ces effets dépendent à la fois de la température et de la gravité. De plus, l'abondance d'hélium a une influence importante sur les effets des métaux ; une abondance d'hélium faible ($\log N(\mathrm{He})/N(\mathrm{H}) \lesssim -1.5$) occasionne des effets assez importants alors qu'une abondance plus élevée tend à réduire ces mêmes effets. Nous avons aussi trouvé que l'ajout du fer (en abondance solaire) ne cause que des changements relativement faibles à la structure en température et, par le fait même, aux profils des raies d'hydrogène et d'hélium, par rapport aux changements déjà produits par le C, N, O (en abondance solaire). Nous avons utilisé nos grilles pour faire une analyse spectroscopique du spectre à haut signal sur bruit (∼180) et basse résolution (9 Å) de SDSS J160043.6+074802.9 obtenu au télescope Bok. Notre meilleure ajustement a été obtenu avec notre grille de spectres synthétiques incluant C, N, O et Fe en quantité solaire, menant aux paramètres suivants : $T_{\mathrm{eff}} = 68\ 500 \pm 1770$ K, $\log g = 6.09 \pm 0.07$, and $\log N(\mathrm{He})/N(\mathrm{H}) = -0.64 \pm 0.05$, où les incertitudes proviennent uniquement de la procédure d'ajustement. Ces paramètres atmosphériques, particulièrement la valeur de l'abondance d'hélium, placent notre étoile dans une région où les effets des métaux ne sont pas très marqués.

Mots clés : étoiles : sous-naines - atmosphères - paramètres fondamentaux - spectroscopie - étoiles : individuelles : SDSS J160043.6+074802.9

Abstract

We present our new grids of model atmospheres and spectra for hot subdwarf O (sdO) stars : standard NLTE H+He models with no metals, NLTE line-blanketed models with C+N+O, and NLTE line-blanketed models with C+N+O+Fe. Using hydrogen and helium lines in the optical range, we make detailed comparisons between theoretical spectra of different grids in order to characterize the line blanketing effects of metals. We find these effects to be dependent on both the effective temperature and the surface gravity. Moreover, we find that the helium abundance also influences in an important way the effects of line blanketing on the resulting spectra : a low helium abundance ($\log N(\mathrm{He})/N(\mathrm{H}) \lesssim -1.5$) leads to relatively large effects, while a high helium abundance tends to reduce their magnitudes. We also find that the addition of Fe (solar abundance) leads only to incremental effects on the atmospheric structure and, hence, on the model line profiles of H and He as compared to the case where the metallicity is defined by C+N+O (solar abundances). We use our grids to perform fits on a 9 Å resolution, high S/N (∼180) optical spectrum of SDSS J160043.6+074802.9, this (currently) unique pulsating sdO, that we gathered at the Bok Telescope. Our best and most reliable result is based on the fit achieved with NLTE synthetic spectra that include C, N, O, and Fe in solar abundances, leading to the following parameters : $T_{\mathrm{eff}} = 68\ 500 \pm 1770$ K, $\log g = 6.09 \pm 0.07$, and $\log N(\mathrm{He})/N(\mathrm{H}) = -0.64 \pm 0.05$ (formal fitting errors only). This combination of parameters, particularly the comparatively high helium abundance, implies that line blanketing effects due to metals are not very large in the atmosphere of this sdO star.

Subject headings : stars : subdwarf - atmosphere - fundamental parameters - spectroscopy - stars : individual : SDSS J160043.6+074802.9

Table des matières

Table des figures

Liste des tableaux

Chapitre 1

Introduction

1.1 Les sous-naines chaudes

Les sous-naines chaudes sont des étoiles évoluées, de faible masse ($\sim 0.5\ M_{\odot}$) et compactes dont l'existence est plutôt méconnue, même parmi les astrophysiciens. Elles se séparent en deux classes spectrales : les sdB ont des températures effectives entre 20 000 et 40 000 K et forment une extension de la branche horizontale (HB) que l'on appelle la branche horizontale extrême (EHB). Les sdO ont quant à elles des températures effectives plus grandes que 40 000 K. Dans les deux cas, la gravité de surface, exprimée en logarithme, variera dans l'intervalle $4.8 \lesssim \log g \lesssim 6.4$. Il ne faut pas confondre les sous-naines chaudes avec les sous-naines traditionnelles, dont les températures sont beaucoup plus faibles et qui sont situées en-dessous des étoiles de la séquence principale dans le diagramme HR et qui ne diffèrent de ces dernières que par leur faible métallicité. Les sous-naines chaudes, quant à elles, se situent entre les étoiles chaudes de la séquence principale et la région des naines blanches. Leur découverte remonte aux années 50 (Humason & Zwicky 1947 ; Iriarte & Chavira 1957 ; Chavira 1958) lors d'un relevé d'étoiles bleues de faible luminosité à haute latitude galactique. Un système de classification spectrale fut rapidement mis au point par Feige (1958) qui classifiait les étoiles bleues dont le spectre ne montrait que des raies de Balmer peu profondes comme des sdB alors que les spectres présentant de fortes raies d'hélium (He I et He II) était classifiés comme des sdO. Ce système de classification demeure encore valable aujourd'hui, bien que quelques

"sous-classes" ont été ajoutées entre-temps. Quelques spectres représentatifs de sous-naines chaudes sont présentés à la figure 1.1.

Il est maintenant connu que les sdB sont des étoiles en phase de brûlage central d'hélium tout en étant recouvertes d'une enveloppe d'hydrogène trop mince pour en permettre le brûlage en couche. Cette enveloppe agit comme un isolant ; plus elle est épaisse moins l'étoile sera chaude. Les étoiles ayant un couche d'hydrogène "normale" (jusqu'à 0.5 $M_{\odot}$) vont former la branche horizontale (HB) alors que les sdB avec leur très mince couche ($\lesssim$ 0.02 $M_{\odot}$) vont en former la partie extrême (EHB) (Heber 2009). Étant donnée cette quantité d'hydrogène anormalement faible, un processus occasionnant la perte d'une partie importante des couches superficielles de l'étoile progénitrice est un élément clé de tout scénario évolutif prétendant expliquer la formation des sdB.

Le modèle d'évolution canonique présenté initialement par Faulkner (1972) propose que les sdB ont des progéniteurs qui perdent tellement de masse près du sommet de la branche des géantes rouges (lorsque le coeur atteint la masse requise pour le flash d'hélium) qu'elles vont se retrouver à l'extrémité chaude de la HB. Ce processus requiert toutefois une masse assez précise du coeur d'hélium (entre 0.46 et 0.5 $M_{\odot}$) permettant l'allumage dans des conditions dégénérées. Pendant longtemps le problème fut de trouver une explication plausible à l'importante perte de masse durant la phase géante rouge permettant la production de sdB. Ce n'est que plusieurs années plus tard que des simulations ont réussi à exliquer assez naturellement ce phénomène (D'Cruz et al. 1996, Sweigart 1997). Les sdB poursuivent une évolution post-EHB lorsque le combustible central s'épuise et que l'hélium se met à brûler en couche. Si la masse de l'enveloppe est suffisamment élevée, l'étoile rejoindra alors la branche asymptotique des géantes (AGB). Toutefois l'enveloppe étant peu importante au départ, elle sera rapidement consumée et l'étoile rejoindra la séquence de refroidissement des naines blanches avant la phase des pulses thermiques. Si la masse de l'enveloppe est trop faible, celle-ci demeurera inerte et l'étoile rejoindra tout simplement la séquence des naines blanches. Ce dernier chemin évolutif passe dans la région des sdO et connecte naturellement les sdO pauvres en hélium aux sdB.

L'existence des sdB peut aussi s'expliquer par l'évolution de systèmes binaires particuliers. Un premier cas serait la fusion de deux naines blanches dont au moins une possède un coeur

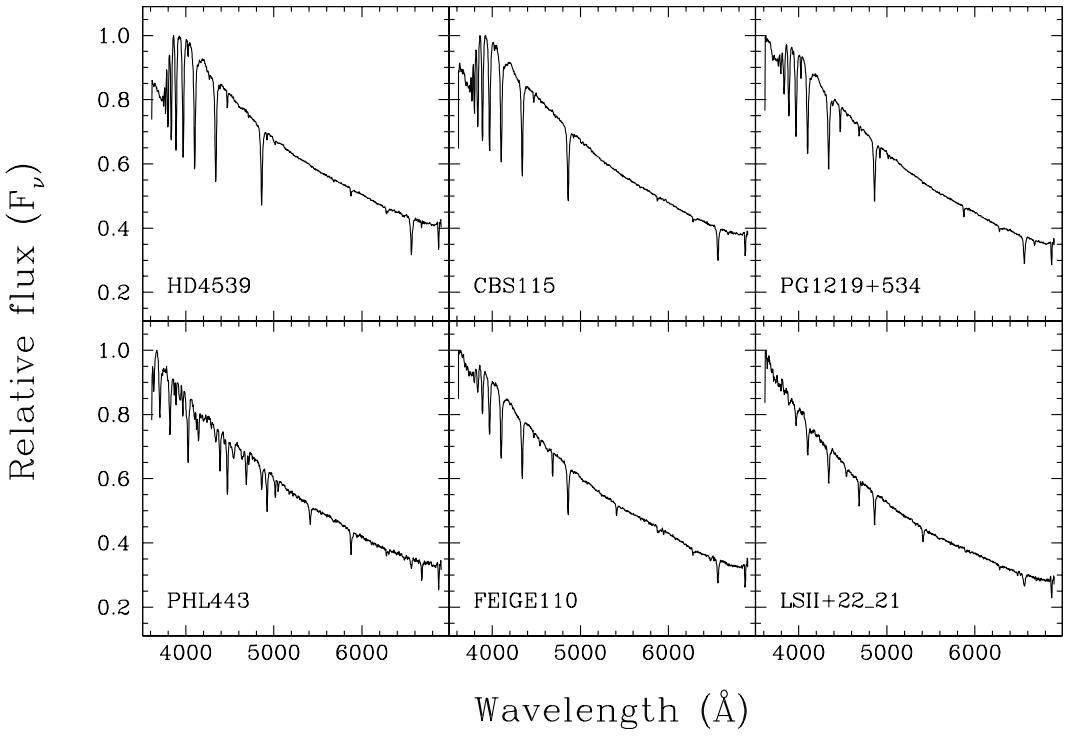

FIGURE 1.1 – Exemples de spectres d'étoiles sous-naines chaudes : les trois spectres du haut proviennent de sdB alors que ceux du bas proviennent de sdO. HD4539 et CBS115 sont des sdB typiques ($T_{\rm eff} \sim 26\ 000$, $\log g \sim 5.3$ et $\log N({\rm He})/N({\rm H}) \sim -2.4$.) montrant de fortes raies de Balmer et de faibles raies d'He I tandis que PG1219+534 est une sdB plus chaude (34 060 K) ayant une abondance d'hélium plus élevée ($\log N({\rm He})/N({\rm H}) = -1.5$). Les raies d'hélium sont plus prononcées dans le spectre de cette dernière, si bien qu'elle fait partie d'une "sous-classe" qu'on appelle sdOB qui regroupent les sdB les plus chaudes présentant de faibles raies d'hélium ionisé. PHL443 est une sdO riche en hélium ($T_{\rm eff} = 41\ 720$ K, $\log g = 5.85$ et $\log N({\rm He})/N({\rm H}) = 1.65$) dont le spectre montre un joyeux mélange de raies d'hélium I et II, sans oublier de faibles raies de Balmer. Feige 110 est quant à elle une sdO plus typique, de température effective et gravité similaires à PHL443 mais ayant cette fois-ci une abondance d'hélium plus faible ($\log N({\rm He})/N({\rm H}) = -1.8$), présentant donc des raies d'hélium moins prononcées que les raies de Balmer. LSII+22_21 est une sdO chaude (69 050 K) à l'abondance d'hélium sous-solaire ($\log N({\rm He})/N({\rm H}) = -1.8$).

d'hélium. Si la période initiale du système binaire est suffisamment courte, la perte de moment angulaire orbital à travers l'émission d'ondes gravitationnelles permettra aux deux étoiles de se rapprocher l'une de l'autre jusqu'à fusionner. L'objet résultant pourrait brûler l'hélium en son coeur et devenir une étoile de la EHB. Des simulations par Han et al. (2002) prédisent une distribution de masse assez large ($0.4 - 0.65\ M_{\odot}$) centrée autour de $0.51\ M_{\odot}$. Toutefois, Gourgouliatos & Jeffery (2006) ont démontré qu'en tenant compte de la conservation du moment angulaire, l'étoile résultant d'une telle fusion aurait une vitesse de rotation supérieure à la vitesse de rupture. Dans ce cas, il reste à trouver un mécanisme permettant à l'étoile de se débarrasser de cet excès de moment angulaire.

Deux autres scénarios expliquent quant à eux la présence de sous-naines faisant partie de systèmes binaires (Han et al. 2002 ; 2003). Dans chacun des cas, l'étoile géante rouge (qui deviendra éventuellement la sous-naine) commence à remplir son lobe de Roche alors qu'elle est à la fin de la phase géante rouge. Si le compagnon ne peut accréter toute la masse transférée, le transfert devient dynamiquement instable et il se formera une enveloppe commune englobant les deux compagnons. La friction entre la matière de l'enveloppe et les étoiles amènera celles-ci à se rapprocher l'une de l'autre jusqu'à ce que l'énergie libérée soit assez grande pour éjecter l'enveloppe. Il en résultera un système binaire rapproché (de courte période) composé du coeur de l'étoile géante qui aura perdu presque tout son hydrogène et d'une étoile de la séquence principale. À ce moment, si le coeur de l'étoile géante est assez massif pour que la combustion de l'hélium démarre, il en résultera une sdB. Dans le second cas, le transfert de masse est dynamiquement stable et cessera lorsque que le rayon de l'étoile primaire, et par le fait même son enveloppe d'hydrogène, auront suffisamment diminué. Encore une fois si le coeur de l'étoile géante est suffisamment massif, il en résultera une sdB dans un système binaire à longue période. Selon le ratio initial des masses des deux étoiles, le compagnon du système final pourra être une naine blanche, une étoile de la séquence principale ou une étoile sous-géante. Mentionnons qu'une fraction assez élevée (entre 40 et 60 % selon les études) des sdB résiderait à l'intérieur de systèmes doubles (Green et al. 1997 ; Maxted et al. 2001 ; Napiwotzki et al. 2004 ; Morales-Rueda et al. 2006) d'où l'importance d'avoir des scénarios évolutifs menant à la formation de tels systèmes.

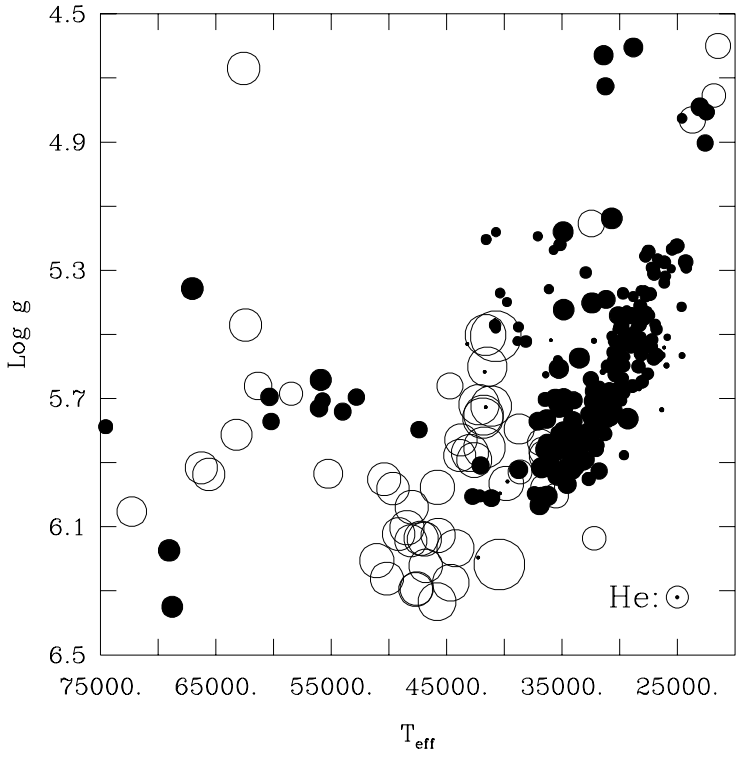

FIGURE 1.2 – Distribution de sous-naines dans le plan log $g - T_{\rm eff}$. La dimension des cercles est une mesure logarithmique de l'abondance d'hélium (log N(He)/N(H)) : une abondance d'hélium plus faible que l'abondance solaire est représentée par un cercle noir alors que les cercles vides représentent une abondance d'hélium plus grande que celle du soleil. On remarque facilement le regroupement des sdB pauvres en hélium sur la EHB, ainsi que quelques sdB riches en hélium, faisant exception à la règle, à la limite des hautes température ($\sim$ 40 000 K). On distingue aussi l'agglomération des sdO riches en hélium entre 40 000 K et 50 000 K tout comme la dispersion plus importante des sdO pauvres en hélium.

Alors que les sdB forment un ensemble assez homogène d'étoiles sur la EHB, les sdO forment une famille d'étoiles plus diversifiées, surtout en terme de composition chimique (voir la figure 1.2). On les sépare en deux "sous-classes" : les sdO riches en hélium (lorsque l'abondance d'hélium est plus grande que l'abondance solaire, soit log N(He)/N(H) ≥ -1.0) et les sdO pauvres en hélium (lorsque l'abondance est sous-solaire). Des études récentes (Napiwotzki 2008, Stroeer et al. 2007) ont montré que ces deux sous-classes semblent avoir des caractérisques bien distinctes. Dans leur échantillon de sdO observées dans le cadre du programme SPY (ESO supernova Ia progenitor survey), Stroeer et al. (2007) ont observé des raies de carbone

ou d'azote dans la portion visible des spectres de toutes leur sdO riches en hélium alors qu'aucune raie de ces éléments n'a été observée dans les étoiles pauvres en hélium. De plus, ces deux sous-classes tendent à se distribuer de façon différente dans le plan $T_{\rm eff}$ − log g : les étoiles riches en hélium se retrouvent majoritairement entre des température de 40 000 K et 50 000 K et des gravités (log g) de 5.5 et 6.3 bien que quelques unes soient en dehors de ces limites (Hirsch et al. 2008). Quant aux étoiles pauvres en hélium, elles sont répandues de façon beaucoup plus uniforme à travers les gammes de températures (jusqu'à 80 000 K) et de gravités des sdO, bien que peu d'entre elles aient des gravités supérieures à 5.8.

Ceci suggère des chemins évolutifs différents pour ces deux sous-classes. Plusieurs hypothèses ont été émises et testées dans le passé, dont quelques unes semblent assez prometteuses. Parmi les différents scénarios évolutifs de systèmes binaires, la fusion de deux étoiles naines blanches à coeur d'hélium pourrait aussi expliquer la formation de sdO riches en hélium (Saio & Jeffery 2000). Ce scénario est toutefois aux prises avec la faiblesse mentionnée précédemment à propos de la perte de moment angulaire encore inexpliquée. L'autre chemin évolutif pouvant mener à la formation de sdO riches en hélium est le "hot-flasher scenario" (Sweigart et al. 1997). Si une quantité assez importante de masse est perdue sur la RGB, le flash d'hélium peut avoir lieu lorsque l'étoile a déjà quittée la branche des géantes rouges. Ce modèle explique bien la composition chimique de l'atmosphère mais reproduit plutôt mal la distribution des étoiles dans le diagramme $T_{\rm eff}$ − log g (Lanz et al. 2004 ; Stroeer et al. 2007). Pour ce qui est des sdO pauvres en hélium, la plupart d'entre elles sont bien expliquées par l'évolution post-EHB mentionnée précédemment alors que les plus lumineuses (température élevée et gravité de surface plus faible), s'expliquent par l'évolution post-AGB d'étoiles peu massives (Napiwotzki 2008).

1.2 Variations de luminosité chez des sous-naines

C'est en 1996 au South African Astronomical Observatory (SAAO) que des variations de luminosité dans des étoiles sous-naines de type B ont été observées pour la première fois (Kilkenny et al. 1997 ; Koen et al. 1997 ; O'Donoghue et al. 1997 ; Stobie et al. 1997). Par une heureuse coïncidence, à la même époque des études théoriques ont été menées (Charpinet et

al. 1996) conduisant à la prédiction de ces variations rapides de luminosité dans des étoiles sdB. Avec des outils théoriques déjà en place, un nouveau sous-domaine d'étude s'est rapidement développé, soit l'astérosismologie des sous-naines chaudes. Le phénomène responsable de l'instabilité causant les pulsations dans les sous-naines s'avère être une forte augmentation de l'opacité située dans l'enveloppe de l'étoile. Ce pic d'opacité est dû à une région d'ionisation partielle d'éléments lourds (principalement le fer). Toutefois, une quantité *locale* très grande de métaux (de 50 à 100 fois l'abondance solaire) est nécessaire afin de produire l'opacité requise pour exciter les modes de pulsations. Cette grande accumulation locale de métaux est possible via le phénomène de lévitation radiative dans ces étoiles. Chayer et al. (1996) ont démontré qu'à certains endroits dans l'enveloppe de ces étoiles, la pression de radiation est suffisamment élevée pour contrebalancer les effets de la gravité chez certaines espèces atomiques. Le fer étant particulièrement sensible à la pression de radiation, il s'accumule dans certaines régions, occasionnant de grandes surabondances locales responsables de l'excitation des modes de pulsations.

L'astérosismologie est un outil sans pareil pour sonder les propriétés internes d'une étoile. Un modèle sismique théorique permet de prédire des périodes d'oscillations bien précises selon la gravité, la température, la masse totale de l'étoile et l'épaisseur de sa couche d'hydrogène. Si on arrive à bien faire concorder des périodes théoriques avec des périodes observées, on obtient alors de précieuses informations sur l'étoile en question. En connaissant les 4 paramètres mentionnés précédemment, il est possible de déduire d'autres propriétés telles que le rayon, la luminosité totale, la magnitude absolue et la distance de l'étoile.

Les premières sous-naines pulsantes découvertes montraient toutes plusieurs périodes d'oscillations assez courtes (entre 80 et 500 secondes) qu'on appelle aussi modes p et qui sont associés à des ondes de pression. On désigne généralement ces étoiles comme des pulsateurs rapides. Quelques années après leur découverte, un second type de pulsations a été observé dans des sdB (Green et al. 2003). Cette fois-ci il s'agissait de variations de luminosité sur de plus longues périodes (2000 à 9000 s) associées à des ondes de gravité (modes g). Des courbes de lumières typiques de ces deux types de pulsateurs sont présentées à la figure 1.3. Ces deux types de pulsateurs se répartissent dans des régions assez bien définies du plan

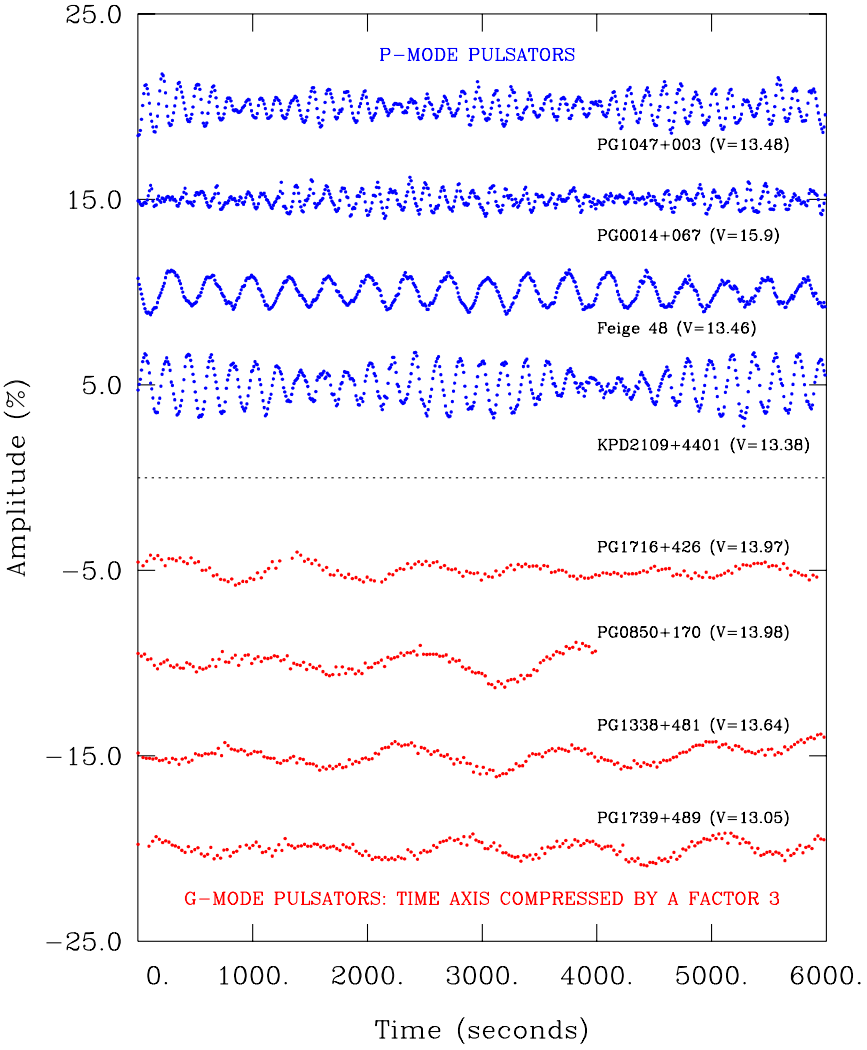

FIGURE 1.3 – Exemple de courbes de lumière représentatives des sdB pulsantes : le panneau du haut montre les variations de luminosité de pulsateurs rapides présentant des modes p alors que le panneau du bas montre des variations de lumière dues aux modes g des pulsateurs lents. Figure tirée de Fontaine et al. (2006).

$T_{\rm eff}-\log g$, les pulsateurs de courtes périodes vont se retrouver entre 28 000 et 37 000 K et $5.25 \lesssim \log g \lesssim 6.00$ tandis que les étoiles ayant des longues périodes seront typiquement plus froides (entre 23 000 K et 28 000 K) et moins compactes. Ces deux régions d'instabilité partagent une frontière commune (voir figure 1.4) où se trouvent des pulsateurs qu'on appelle hybrides, c'est-à-dire, montrant à la fois des modes p et des modes g. La découverte de la première étoile de ce type, HS 0702+6043 (Schuh et al. 2006), a eu lieu quelques années après la découverte des pulsateurs lents. Depuis cette première découverte, 3 autres étoiles se sont ajoutées au lot (Oreiro et al. 2005 ; Lutz et al. 2008 ; Baran & Fox-Machado 2009). On connaît maintenant plus de 70 sous-naines pulsantes, et une dizaine de nouveaux cas ont récemment été découverts par le satellite Kepler (Østensen et al. 2010).

Il n'a été question jusqu'à maintenant que de sous-naines pulsantes de type B. Après leur découverte, des efforts ont été faits afin de trouver cette fois-ci des sdO pulsantes, tout en tentant de réaliser théoriquement des modèles astérosismologiques de ces étoiles (Rodríguez-López et al. 2007 ; 2008). C'est encore une fois par hasard, qu'en 2006 au SAAO la première (et aujourd'hui encore la seule) sdO pulsante, SDSS J1600+0748, fut observée dans le cadre d'une campagne de recherche d'étoiles variables cataclysmiques de type AM CVn (Woudt et al. 2006). Le spectre obtenu révéla qu'il s'agissait vraisemblablement d'un système binaire composé d'une sdO et d'une étoile de la séquence principale.

1.3 Le cas de SDSS J1600+0748

Suite à la découverte de Woudt et al. (2006), d'autres efforts ont été mis en oeuvre par Fontaine et al. (2008) afin de présenter une analyse préliminaire, quoique assez complète, de cette unique sdO pulsante. Tout d'abord, un spectre à basse résolution (9 Å) et haut signal sur bruit (∼180) de SDSS J1600+0748 a été obtenu au télescope de 2.3 m du Steward Observatory. Plusieurs spectres d'étoiles de la séquence principale (F, G, K), obtenus avec les mêmes instruments, ont ensuite été testés afin de trouver le type spectral le plus probable du compagnon, menant à une étoile de type G0V. En soustrayant un spectre de G0V au spectre de SDSS J1600+0748, il est possible de "nettoyer" le spectre observé de la lumière du compagnon afin de garder uniquement la composante spectrale correspondant à la sous-naine (plus

de détails sur ces procédures sont inclus à l'Annexe A). Une analyse spectroscopique du spectre nettoyé a conduit aux paramètres suivants : $T_{\rm eff}$= 71 070 ± 2725 K, log g = 5.93 ± 0.11 et log N(He)/N(H) = −0.67 ± 0.08. Par la suite, en utilisant la température et la gravité déterminées spectroscopiquement, combinées avec des masses typiques pour l'étoile et sa couche d'hydrogène, les auteurs ont réussi à faire un modèle astérosismologique, en incluant la lévitation radiative, reproduisant bien la gamme de périodes de pulsations observées dans l'étoile.

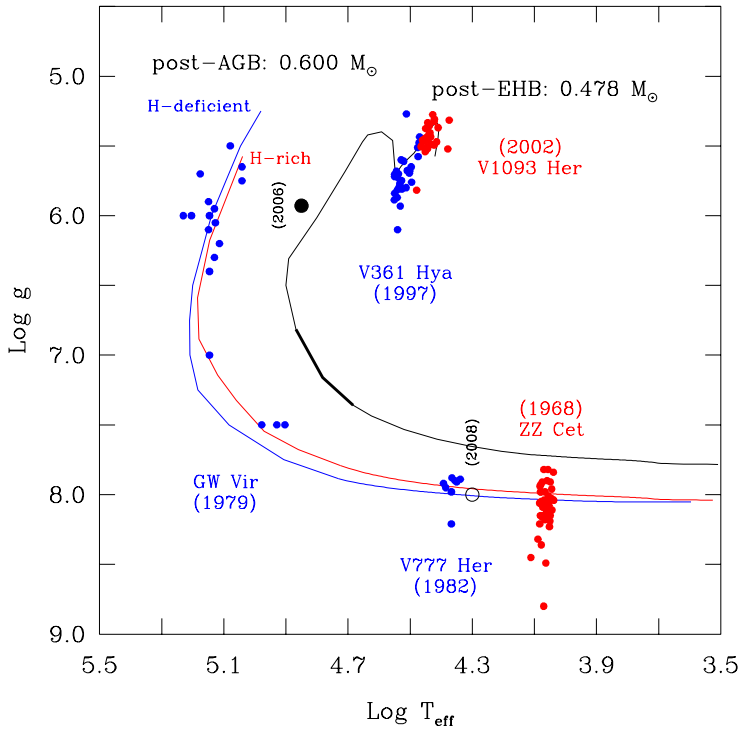

FIGURE 1.4 – Cette figure montre la position dans le diagramme HR spectroscopique des différents types de pulsateurs compact connus. On peut facilement voir les sdB pulsantes se diviser en deux sous-catégories selon le type de pulsations, dont les nomenclatures officielles de l'Union Astronomique Internationale sont V361 Hya pour les pulsateurs rapides et V1093 Her pour les pulsateurs lents. Le point noir (2006) indique la position de J1600+0748, encore aujourd'hui la seule sdO pulsante connue. Parmis les types récemment découverts on compte aussi les étoiles naines blanches pulsantes à atmosphère de carbone (cercle vide indiqué 2008) dont quatre membres sont maintenant connus.

Le projet effectué dans le cadre de cette maîtrise concerne de près cette étoile particulière qu'est SDSS J1600+0748. Une difficulté des analyses astérosismologiques est qu'elles mènent

souvent à plus d'une solution pouvant reproduire les observations. On se retrouve ainsi avec une dégénérescence que l'on arrive à lever à l'aide d'une détermination indépendante et précise de la température effective et de la gravité par analyse spectroscopique.

L'analyse spectroscopique de Fontaine et al. (2008) a été faite en utilisant une grille de modèles d'atmosphères hors équilibre thermodynamique local (Hors-ETL) incluant de l'hydrogène et de l'hélium. Chaque modèle de la grille est défini en fonction de sa température effective, sa gravité et son abondance d'hélium. Ces paramètres vont déterminer la structure en température et en pression de l'atmosphère de l'étoile, déterminant ainsi la distribution spectrale de la lumière émergente.

Étant donné que SDSS J1600+0748 est une étoile très chaude, l'approximation de l'équilibre thermodynamique local ne s'applique pas et c'est pourquoi il faut avoir recours aux modèles d'atmosphères hors-ETL. Ces modèles sont plus précis mais demandent beaucoup plus de temps de calcul que lorsqu'on utilise l'approximation ETL. Bien que le spectre visible de l'étoile ne montre pas de raies métalliques, il n'en demeure pas moins qu'elle contient sans aucun doute des éléments lourds dans son atmosphère. Plusieurs études ont montré que l'inclusion d'éléments lourds dans les modèles d'atmosphères Hors-ETL de sdO peut avoir un effet considérable sur le spectre émergent de l'étoile et donc influencer les paramètres atmosphériques obtenus lors d'une analyse spectroscopique (Dreizler & Werner 1996 ; Haas et al. 1996 ; Lanz et al. 1997 ; Rauch 2000). L'ajout de métaux dans l'atmosphère aura des effets importants sur la structure en température, les couches internes vont se réchauffer alors que la température de surface peut chuter de quelques dizaines de milliers de Kelvin. Selon leur région de formation, les raies spectrales seront affectées différemment par le changement de température occasionné par la présence de métaux. Un problème récurrent dans le cas des étoiles chaudes est ce qu'on appelle le "problème des raies de Balmer" (voir Bergeron et al. 1993). Ces fortes raies d'hydrogène dans le domaine optique sont couramment utilisées pour déterminer la température effective et la gravité d'une étoile. Dans le cas des étoiles chaudes, comme les sdO, le problème vient de l'impossibilité d'obtenir un ajustement convenable pour toutes les raies de la série simultanément. En fait, en ajustant individuellement les raies de Balmer, on trouve des différences de température allant jusqu'à un facteur 2 par exemple,

entre les températures obtenues avec Hα et Hδ (Napiwotzki 1993 ; Werner 1996). Puisque ces raies se forment à des profondeurs légèrement différentes, de plus en plus grandes à mesure que l'on augmente dans la série, le problème des raies de Balmer vient donc d'une structure en température erronnée. Traiter la présence des métaux de façon réaliste dans les modèles d'atmosphères est un élément clé pour obtenir les conditions physiques permettant de reproduire correctement les observations de spectres d'étoiles chaudes.

Or, le problème majeur de l'inclusion de métaux dans les modèles est l'augmentation très rapide du temps de calcul à mesure que des espèces atomiques possédant plusieurs niveaux d'énergie chacune sont ajoutées. C'est pourquoi des calculs de grilles de modèles d'atmosphères Hors-ETL *avec* métaux pour des sdO n'ont pas été réalisés dans le passé (mentionnons toutefois que de telles grilles ont été réalisées pour des étoiles O et B de la séquence principale par Lanz & Hubeny (2003 ; 2007)). Les quelques études qui ont été faites impliquaient seulement un nombre restreint de modèles (moins d'une dizaine). Ce que nous proposons de faire pour ce projet est justement de calculer des grilles complètes de modèles d'atmosphères HETL avec métaux pour des étoiles sdO. Cela sera possible dans un intervalle de temps raisonnable grâce au travail de M. Pierre Brassard qui a adapté les codes publics TLUSTY et SYNSPEC, utilisés respectivement pour calculer des modèles d'atmosphères et des spectres synthétiques, pour les exécuter en parallèle sur un réseau de 80 processeurs récemment acquis par notre groupe de recherche. Nos grilles couvrent un intervalle de température allant de 60 000 à 80 000 K puisque notre but est d'obtenir un meilleur ajustement que celui de Fontaine et al. (2008) pour SDSS J1600+0748 (dont la température est, rappelons-le, $\sim$ 70 000 K). Nous couvrons aussi des intervalles de gravité allant de 4.8 à 6.4 (en log g) et d'abondance d'hélium entre 0.0 et -4.0, exprimé en log $N(\mathrm{He})/N(\mathrm{H})$.

Notre première grille est composée de modèles traditionnels incluant l'hydrogène et l'hélium. Dans notre seconde grille, du carbone, de l'azote et de l'oxygène en abondance solaire sont ajoutés, étant donné que nous n'avons, de prime abord, aucune indication quant à l'abondance de ces éléments dans notre étoile. Notre troisième grille contient, en plus des éléments mentionnés précédemment, du fer à 1/10 de l'abondance solaire et a principalement servi d'intermédiaire pour la quatrième grille contenant cette fois-ci du fer en abondance solaire. En déter-

minant les paramètres atmosphériques ($T_{\rm eff}$, log g et log N(He)/N(H)) de SDSS J1600+0748 avec nos différentes grilles, on s'attend à obtenir des valeurs différentes tout en reproduisant mieux certaines raies d'absorption (Hβ, Hγ, He II 4686 et He II 5412) qui pour l'instant (avec les modèles sans métaux) ne sont pas assez profondes. Ces différences nous donneront une idée des effets que les métaux peuvent avoir dans le cas de SDSS J1600+0748. Cependant, ces effets peuvent potentiellement varier selon la température, la gravité et l'abondance d'hélium dans l'atmosphère. Nous utiliserons donc aussi les modèles de nos différentes grilles afin de quantifier ces effets sur la gamme de paramètres atmosphériques couverte par nos grilles.

Chapitre 2

NLTE Model Atmospheres and Spectra for Hot O Subdwarfs : An Application to the Pulsating Star SDSS J160043.6+074802.9

M. Latour[1], G. Fontaine[1], P. Brassard [1], E. M. Green [2], P. Chayer [3], S. K. Randall [4]

To be submitted to *The Astrophysical Journal*

September 2010

1. Département de physique, Université de Montréal, C.P. 6128, Succursale Centre-Ville, Montréal, QC H3C 3J7, Canada

2. Department of Astronomy and Steward Observatory, University of Arizona, 933 North Cherry Avenue, Tucson, AZ 85721, USA

3. Space Telescope Science Institute, 3700 San Martin Drive, Baltimore, MD 21218, USA

4. ESO, Karl-Schwarzschild-Str. 2, 85748 Garching bei München, Germany

2.1 Abstract

We present our new grids of model atmospheres and spectra for hot subdwarf O (sdO) stars : standard NLTE H+He models with no metals, NLTE line-blanketed models with C+N+O, and NLTE line-blanketed models with C+N+O+Fe. Using hydrogen and helium lines in the optical range, we make detailed comparisons between theoretical spectra of different grids in order to characterize the line blanketing effects of metals. We find these effects to be dependent on both the effective temperature and the surface gravity. While the neglect of metal blanketing leads to systematic underestimates of the true values of the surface gravity in the ranges covered by our grids, the response is not monotonic for the effective temperature. Moreover, we find that the helium abundance also influences in an important way the effects of line blanketing on the resulting spectra : a low helium abundance ($\log N(\mathrm{He})/N(\mathrm{H}) \lesssim -1.5$) leads to relatively large effects, while a high helium abundance tends to reduce their magnitudes. We also find that the addition of Fe (solar abundance) leads only to incremental effects on the atmospheric structure and, hence, on the model line profiles of H and He as compared to the case where the metallicity is defined by C+N+O (solar abundances). We use our grids to perform fits on a 9 Å resolution, high S/N (∼180) optical spectrum of SDSS J160043.6+074802.9 that we gathered at the Bok Telescope. Given that the target is an unresolved binary star, we spent efforts to separate the contribution of the hot O subdwarf from that of its companion, which we tentatively identify as a G0V star. Fortunately, the exact nature of the companion does not affect very significantly the inferred atmospheric parameters of the sdO component which, as its sole member, currently defines the class of pulsating hot O subdwarfs. Although less useful because of their more limited S/N, we also consider two other spectra, one gathered at the New Technology Telescope, and the other taken from the SDSS archives. Our best and most reliable result is based on the fit to the Bok spectrum achieved with NLTE synthetic spectra that include C, N, O, and Fe in solar abundances, leading to the following parameters for the pulsating component : $T_{\mathrm{eff}} = 68\ 500 \pm 1770$ K, $\log g = 6.09 \pm 0.07$, and $\log N(\mathrm{He})/N(\mathrm{H}) = -0.64 \pm 0.05$ (formal fitting errors only). This combination of parameters, particularly the comparatively high helium abundance, implies that line blanketing effects due to metals are not very large in the atmosphere of this sdO

star. We thus find that our derived atmospheric parameters are relatively secure, even though the true metallicity is still unknown. These fortunate circumstances strengthen the pulsational analysis carried out by Fontaine et al. (2008) on this interesting star.

Keywords : stars : atmospheres - stars : fundamental parameters - stars : subdwarfs stars : individual (SDSS J160043.6+074802.9)

2.2 Introduction

SDSS J160043.6+074802.9 (hereafter J1600+0748) is this unique hot subdwarf O (sdO) star showing short-period pressure-mode instabilities. It currently defines by itself the class of pulsating sdO stars, one of the seven distinct families of compact pulsators presently known (see, e.g., Fontaine & Brassard 2008). Its variability as well as its spectral type were uncovered during the course of a search for new AM CVn stars carried out by Woudt et al. (2006). Although these investigators did not provide estimates of the atmospheric parameters of J1600+0748, the SALT spectrum that they gathered leaves little doubt that it is an unresolved noninteracting spectroscopic binary consisting of a very hot sdO subdwarf and late-type main sequence companion. The variability of J1600+0748 is characterized by several very rapid oscillations covering a range of periods from about 60 s to about 120 s, and with amplitudes ranging from ∼0.005 mag to ∼0.040 mag. For several reasons, it is best explained in terms of pulsational instabilities in the sdO primary. Its discovery came as a real surprise to the asteroseismology community, given that a previous stability survey of models of sdO stars did not suggest the existence of rapid pulsations in these objects (Rodríguez-López et al. 2006).

The puzzling existence of oscillations in J1600+0748 was subsequently explained by Fontaine et al. (2008) who demonstrated that radiative levitation, not considered by Rodríguez-López et al. (2006), is the key physical mechanism behind the pulsations. There is enough flux in a hot star such as J1600+0748 to support locally, specifically in the driving region, an abundance of Fe more than 100 times its normal solar value. This dramatically increases the

opacity in that region, and induces pulsational instabilities through the classic κ-mechanism, an effect that is not present in uniform-metallicity models. Hence, the observed luminosity variations in J1600+0748 are naturally explained in terms of radiative levitation which leads to the excitation of low-order, low-degree pressure modes with the appropriate periods.

This small success was based, in part, on a preliminary analysis of an excellent low-resolution optical spectrum of J1600+0748 that one of us (E.M.G.) gathered at the 2.3-m Bok Telescope at Steward Observatory. Serious efforts were invested in the determination and gathering of appropriate spectral templates to represent the main-sequence companion. The latter was ultimately identified as a G0V star, and the observed spectrum was "cleansed" of the polluting light of that star. The analysis of the cleansed spectrum presented in Fontaine et al. (2008) was based on a grid of NLTE model atmospheres and synthetic spectra, but with compositions containing only H and He and no other heavier elements. This led to the first quantitative estimates of $T_{\rm eff}$ = 71,070 $\pm$ 2725 K, log g = 5.93 $\pm$ 0.11, and log N(He)/N(H) = $-$0.65 $\pm$ 0.08 (errors of the fit only) for the atmospheric parameters of J1600+0748 [5]. Those were found to be compatible with the observed pulsation periods in J1600+0748 in conjunction with the predictions of nonadiabatic pulsation theory as described in Fontaine et al. (2008). In the meantime, we recalibrated the Bok spectrum and we further exploit it below.

An independent spectroscopic analysis of J1600+0748 has been recently presented by Rodríguez-López et al. (2010), using the archived SDSS spectrogram as observed data and NLTE H+He theoretical models. These authors adopted a rather ambitious approach and attempted to derive simultaneoulsy nine parameters that define the binary system, including radial velocities, solid angles, and interstellar reddening, along with the usual atmospheric parameters of the two components. They inferred a later spectral type for the companion, namely K3V, than what we deduce from our Bok spectrum. Of more direct interest for the present discussion, they obtained the following estimates for the atmospheric parameters of the sdO component : $T_{\rm eff}$ = 70,000 $\pm$ 5 000 K, log g = 5.25 $\pm$ 0.30, and log N(He)/N(H) = $-$0.51 $\pm$ 0.16 (formal fitting errors). We find it encouraging that the values of the effective temperature and

5. There is a misprint in Fontaine et al. (2008) in that the reported value of the helium abundance, log N(He)/N(H) = $-$0.85 $\pm$ 0.08, should have been $-$0.65 $\pm$ 0.08.

the helium abundance obtained by Rodríguez-López et al. (2010) are consistent with those derived previously by Fontaine et al. (2008). However, their estimate of the surface gravity is significantly lower than that of Fontaine et al. (2008). We have to point out, in this context, that the value $\log g = 5.25 \pm 0.30$ obtained by Rodríguez-López et al. (2010) is too low to be compatible with nonadiabatic pulsation theory and the observed period range in J1600+0748.

These two studies of J1600+0748 used theoretical model atmospheres including only hydrogen and helium, while this star likely contains its fair share of metals (currently in unknown abundances and proportions). We thus felt it was important to assess the role of such metals on its derived atmospheric parameters and hopefully pin down better its position in the surface gravity-effective temperature plane. The determination of reliable atmospheric parameters for this star is particularly important in order to constrain an eventual seismic model. We emphasize the significance of this in a broader context since a successful seismic analysis of J1600+0748 would allow the probing of a new and totally different evolutionary phase than has been possible so far with compact pulsators. Beyond this specific application, we also felt that a more general study of the properties of hot sdO model spectra including the presence of metals would be worthwhile and timely, given the current unavailability of large grids for such models.

With these ideas in mind, we constructed several grids of model atmospheres and synthetic spectra suitable for the analysis of the optical spectrum of J1600+0748. Preliminary results were discussed in Latour et al. (2010) and, in this paper, we present our complete study. We first discuss at some length our latest grids of NLTE metal line-blanketed model atmospheres and synthetic spectra in §2. This includes detailed comparisons between the various grids in order to illustrate clearly NLTE and line-blanketing effects on the model spectra. We next present in §3 the observational material that we have available on J1600+0748, and we discuss the results of our spectral analysis of this material using our new model grids. We summarize our findings in the last section.

2.3 Model atmospheres and synthetic spectra

2.3.1 Some Background

It is well known that the assumption of local thermodynamic equilibrium (LTE) is inappropriate in the case of hot evolved objects such as sdO stars because, primarily, of their high surface temperatures (see, e.g., Dreizler & Werner 1993 and references therein). Exact non-LTE (NLTE) calculations are therefore required if one wants to compute realistic model atmospheres for these stars. Unfortunately, such models are much more complicated to compute and require much longer CPU time than their LTE counterparts. This is due to the fact that atomic level populations do not depend only on local pressure and temperature, but are also strongly influenced by the (non-local) radiation field. In turn, this radiation field is a function of temperature and all population densities in each atmospheric layer. The situation becomes particularly complex when one wants to include elements heavier than helium and treat properly the line blanketing ensuing from potentially millions of atomic transitions.

Despite these difficulties, significant breakthroughs have been made since the nineties in the field of the spectral analysis of hot subdwarf stars using model atmospheres that include both deviations from local thermodynamic equilibrium and metal line blanketing. For instance, Dreizler & Werner (1993) were the first to compute NLTE model atmospheres for hot evolved stars including line blanketing of all iron group elements. To handle the growing complexity of model atoms for elements heavier than helium, they constructed a generic ion representing the whole iron group for each ionization stage. Typically, energy levels of a generic ion were grouped into 7 model bands. In this way, they presented the first metal line-blanketed NLTE model atmospheres for O stars, including more than 100,000 lines of elements from scandium through nickel. Their generic ion models were then improved by the addition of theoretically predicted levels by Kurucz (1988) and used for the analysis of the *IUE* spectrum of BD +28°4211, a hot sdO star (Haas et al. 1996). Werner (1996) subsequently emphasized the importance of Stark broadening in the lines of the CNO elements in an improved study of the same star, among other results.

Around the same period, Lanz et al. (1997) constructed NLTE line-blanketed model atmos-

pheres and spectra for the sdO star BD +75°325 using their well-known computer programs TLUSTY and SYNSPEC. In addition to C, N, O, and Si, they included Fe and Ni in their models. They built a model atom for each ionization stage of each element where lower levels are treated individually, while higher ones are regrouped into so-called superlevels. Transitions involving the latter were treated via opacity distribution functions. Their best estimates for the atmospheric parameters of BD +75°325 are $T_{\rm eff}$ = 52,000 K, log g = 5.5, and log N(He)/N(H) = 0.0. In particular, the effective temperature was found a full 6000 K lower than an estimate based on models including only H and He, thus emphasizing the importance of metal line blanketing.

The primary strategy used in these studies (and see Deetjen 2000 and Rauch 2000 for other examples of analyses of sdO stars) was designed to reduce the computing time to acceptable levels. The basic approach has been to predetermine the values of the effective temperature and surface gravity using a grid of NLTE models including hydrogen and helium only. A few models around those values can then be computed with various abundances of metals, thus avoiding the need to have a complete grid of such models. This technique has been used successfully in the past for the spectral analyses of specific sdO stars such as those already cited above. However, large grids of models suitable for the general analysis of other sdO stars have remained unavailable.

It is only in the last decade, when the needed computer resources became largely accessible, that large grids (typically several hundred models) of NLTE model atmospheres and spectra including metals could be realistically envisioned. For instance, Lanz & Hubeny (2003, 2007) provided the first grids of NLTE line-blanketed model atmospheres and spectra for hot stars on the main sequence. They used their codes TLUSTY and SYNSPEC to construct the OSTAR2002 grid (Lanz & Hubeny 2003) composed of 680 models including 11 atomic elements from hydrogen to nickel, and the BSTAR2006 grid (Lanz & Hubeny 2007) composed of 1540 models including the same elements as the first one but with updated atomic data. Rauch (2003) likewise provided a large grid of synthetic ionizing spectra for very hot compact stars. More recently, Gianninas et al. (2010) presented large grids of NLTE model atmospheres including blanketing by C, N, and O suitable for analyzing the spectra of DAO white dwarfs.

2.3.2 Model Grids

Given our interest in the quantitative analysis of the spectrum of the hot sdO component in the J1600+0748 system, we decided to construct appropriate grids of model atmospheres and spectra using the public codes TLUSTY (Version 200) and SYNSPEC (Version 48) made available and maintained by Ivan Hubeny at the University of Arizona and Thierry Lanz at the University of Maryland on their web site[6]. The first computer program, TLUSTY, has been developed initially in the late eighties (Hubeny 1988), and allows the computations of model stellar atmospheres assuming plane-parallel geometry, hydrostatic equilibrium, and thermal equilibrium. Later, the introduction of the hybrid complete linearization/accelerated lambda iteration technique (Hubeny & Lanz 1995) enabled the calculation of "exact" fully line-blanketed NLTE model atmospheres. The second program, SYNSPEC, is used to compute synthetic spectra, given an atmospheric structure.

In order to be able to calculate large grids of models over acceptable timescales ($\lesssim 1$ month of CPU time per grid), one of us (P.B.) invested considerable efforts to adapt the codes TLUSTY and SYNSPEC for them to run in parallel on a cluster of computers. A search strategy in 3D space ($T_{\rm eff}$, log g, and log N(He)/N(H)) was also developed and implemented to ease convergence problems encountered sometimes with TLUSTY, by providing automatically different possible initial models to restart a calculation. In this way, tedious manual interventions to complete a grid calculation were reduced to a minimum. We used CALYS, a small cluster of dedicated PC's built also by P.B. at the Université de Montréal, currently consisting of 80 fast processors. CALYS provided us with a very inexpensive solution to our computing requirements for the needed NLTE models. The same setup was used by our colleagues Gianninas et al. (2010) in their calculations of DAO model atmospheres and spectra.

We have constructed four grids of NLTE model atmospheres defined in terms of 11 values of the effective temperature ($T_{\rm eff}$ from 60,000 K to 80,000 K, in steps of 2000 K), 9 values of the surface gravity (log g from 4.8 to 6.4, in steps of 0.2 dex), and 9 values of the helium-to-hydrogen number ratio (log N(He)/N(H) from -4.0 to 0.0, in steps of 0.5 dex). These grids differ by various metal contents. In addition, for comparison purposes, we also computed a grid

6. http ://nova.astro.umd.edu

TABLE 2.1 – Characteristics of Model Grids

Grid	Type	$\Delta T_{\rm eff}$ (10^3 K)	$\Delta\log g$ (dex)	$\Delta\log N({\rm He})/N({\rm H})$ (dex)	Number of models	Metals (solar)
GHHe	NLTE	60−80, 2	4.8−6.4, 0.2	−4.0−0.0, 0.5	891	...
GHHeCNO	NLTE	60−80, 2	4.8−6.4, 0.2	−4.0−0.0, 0.5	891	C,N,O
GHHeCNOFe0.1	NLTE	60−80, 2	4.8−6.4, 0.2	−4.0−0.0, 0.5	891	C,N,O,Fe(0.1)
GHHeCNOFe	NLTE	60−80, 2	4.8−6.4, 0.2	−4.0−0.0, 0.5	891	C,N,O,Fe
GHHeLTE	LTE	40−70, 2	4.8−6.4, 0.2	−4.0−0.0, 0.5	1584	...

of H+He LTE models defined by 16 values of the effective temperature ($T_{\rm eff}$ from 40,000 K to 70,000 K, in steps of 2000 K), and the same 9 values of the surface gravity and the 9 values of the helium-to-hydrogen number ratio as mentioned just above. The characteristics of these grids are summarized in Table 2.1. Note that grid GHHeCNOFe0.1 was constructed mainly as an intermediate step for the eventual inclusion of iron at full solar abundance. Note also that our grids do not cover the full domain of interest for sdO stars, especially in effective temperature, but they are quite sufficient for the spectral analysis of J1600+0748.

Among the hot sdO stars, there is no known standard atmospheric chemical composition as these objects form a mixed bag of products of post-EHB and post-AGB evolution. Specifically for J1600+0748, there is no hint, in currently available spectra, on which elements (heavier than helium) could be present in its atmosphere, and even less on their abundances. Since our main goal has been to carry out an exploration of the effects of the presence of representative metals on the derived atmospheric parameters for that star, we used in our models typical solar abundances for C, N, O, and Fe, and included only iron among the iron-peak elements. We are aware that these abundances are very likely not the real ones, and that further observations are necessary to get more information about the atomic species present in this star and, thus, perform a self-consistent analysis of J1600+0748. This will have to await the availability of the appropriate data.

The following ions were included in our models : C II to C V, N II to N VI, O II to O VII, and Fe II to Fe VIII. The higher ionization stage of each element is taken as 1-level ion. We used model atoms available on the TLUSTY web site where, for ions of C, N, and O, there are a few models available with different number of levels and superlevels. We took those used in the BSTAR2006 grid from Lanz & Hubeny (2007), except for O VI which was used

only in OSTAR2002 (Lanz & Hubeny 2003), and Fe VII (Lanz, private communication). The radiative transfer equation was solved for up to 11,400 frequency points (in the presence of Fe) and 50 depth points. We did not include any microturbulent velocity, and used opacity sampling to treat line blanketing. Theoretical spectra were then computed with SYNSPEC using discontinuous finite elements to solve the radiative transfer equation. More than 300,000 frequency points were used at that stage, sampling the optical domain from 3500 Å to 6800 Å. Lines were allowed to contribute to the total opacity within a distance of 200 Å from the line center, and we took into account all lines having an opacity (at the center of the line) higher than 10^{-8} times the continuum opacity. We also used detailed Stark profiles (available on the TLUSTY website) for most of the hydrogen and helium lines of interest.

2.3.3 Sample Model Spectra

Figure 2.1 illustrates some model spectra taken from the GHHeCNOFe grid and characterized by $T_{\rm eff}$ = 70,000 K and log g = 6.0. The spectra differ by their different assumed helium-to-hydrogen number ratios. The metal lines are clearly more visible in the He-poor atmospheres than in their more He-rich counterparts. Also, of interest below, we point out here that the strongest metal line in these spectra is an O IV absorption feature at 4632 Å.

Of more direct interest for spectral fitting, Figure 2.2a (2.2b) shows the predicted line profiles of the six lowest hydrogen lines in the Balmer series for representative models with $T_{\rm eff}$ = 70,000 K, log g = 6.0, and log N(He)/N(H) = −0.5 (−2.0). The models are taken from the grids GHHe (blue curves), GHHeCNO (red curves), and GHHeCNOFe (black curves). The presence of metals changes the atmospheric structure and, consequently, the profiles of the Balmer lines. This is particularly evident in the cores of Hα and Hβ, where observations of sufficient resolution would readily reveal that presence. Otherwise, for the other Balmer lines, the models including metals generally predict deeper features.

A comparison of Figure 2.2a with Figure 2.2b indicates that the Balmer lines are stronger in the latter case as a direct result of the larger abundance of hydrogen. In addition, the effects of metals are more obvious in the case illustrated in Figure 2.2b. Hence, in line with our remark just above, the metals are not only more visible directly in model spectra with less helium,

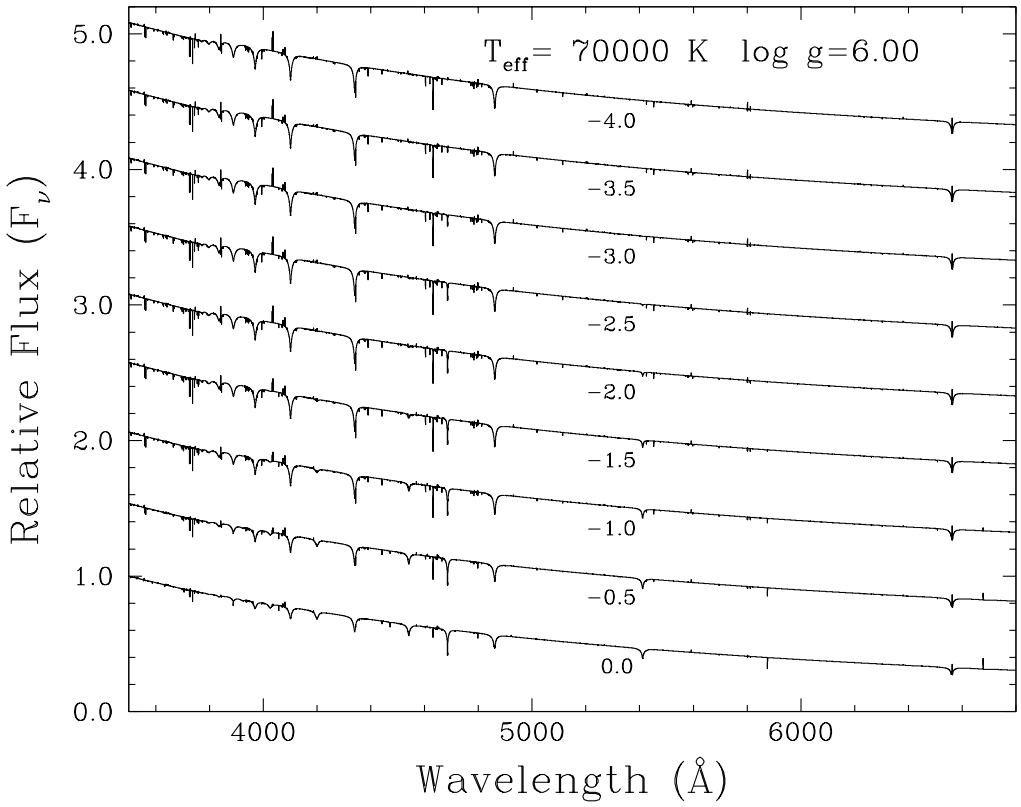

FIGURE 2.1 – Representative synthetic spectra covering the range 3500−6800 Å. The models are defined by the values of $T_{\rm eff}$ = 70,000 K, log g = 6.0, log N(He)/N(H) from −4.0 to 0.0 in steps of 0.5 dex, and a metallicity given by solar abundances of C, N, O, and Fe. The flux is in F_ν units (erg cm^{-2} s^{-1} Hz^{-1}), but the spectra have been normalized at 3500 Å and arbitrarily shifted vertically for visualization purposes. The strongest metallic line is an O IV feature at 4632 Å.

but they also leave stronger signatures on the Balmer line profiles in these spectra. In all cases illustrated in both figures, one can note only very small differences between the profiles predicted in model spectra with C+N+O (red curves) and those based on atmospheres containing C+N+O+Fe (black curves). This indicates that the presence of Fe in solar abundance only leads to small incremental effects on the Balmer line profiles as compared to the case where only C, N, and O are included (again in solar abundances).

We show, in Figures 2.3a and 2.3b, the predicted profiles for several important He lines taken from the same representative model spectra. The larger He abundance in the cases depicted in Figure 2.3a readily explains the much larger line strengths seen there compared to the cases shown in Figure 2.3b. For the two figures, the influence of metals is most obvious in the He II 4686 and 5412 lines. We note again that a high helium abundance tends to mask the presence of metal features. Furthermore, as in the case of the hydrogen Balmer lines, there is only very small differences between the predicted line profiles using models with C+N+O and those obtained with models including C+N+O+Fe.

It is interesting, in the present context, to examine the temperature structures of some representative model atmospheres. For instance, we show in Figure 2.4 the temperature stratifications of three typical models defined by $T_{\rm eff} = 70{,}000$ K, $\log g = 6.0$, and $\log N({\rm He})/N({\rm H}) = -0.5$, but differing by their metal contents. The solid curve (model taken from grid GHHe) exhibits the well-known temperature reversal characteristic of NLTE H+He models with no metals. The dotted curve refers to a model that includes C+N+O (GHHeCNO), and the dashed curve to a model with C+N+O+Fe (GHHeCNOFe). In the latter two cases, the "cooling" effects of the metals in the outer layers of the atmosphere – a well-documented phenomenon – are particularly evident. In the deeper layers, backwarming effects show a monotonic behavior : the more metals, the higher the temperature at a given depth. We note also that the temperature distributions do not differ very much for the two models with metals, underlining, once again, the small incremental contribution of Fe.

We also added in Figure 2.4 the monochromatic optical depth $\tau_\nu = 2/3$ distribution as a function of depth for the GHHeCNOFe model. The equivalent distributions for the two other models are very similar and, consequently, are not shown here. The $\tau_\nu = 2/3$ curve is instructive

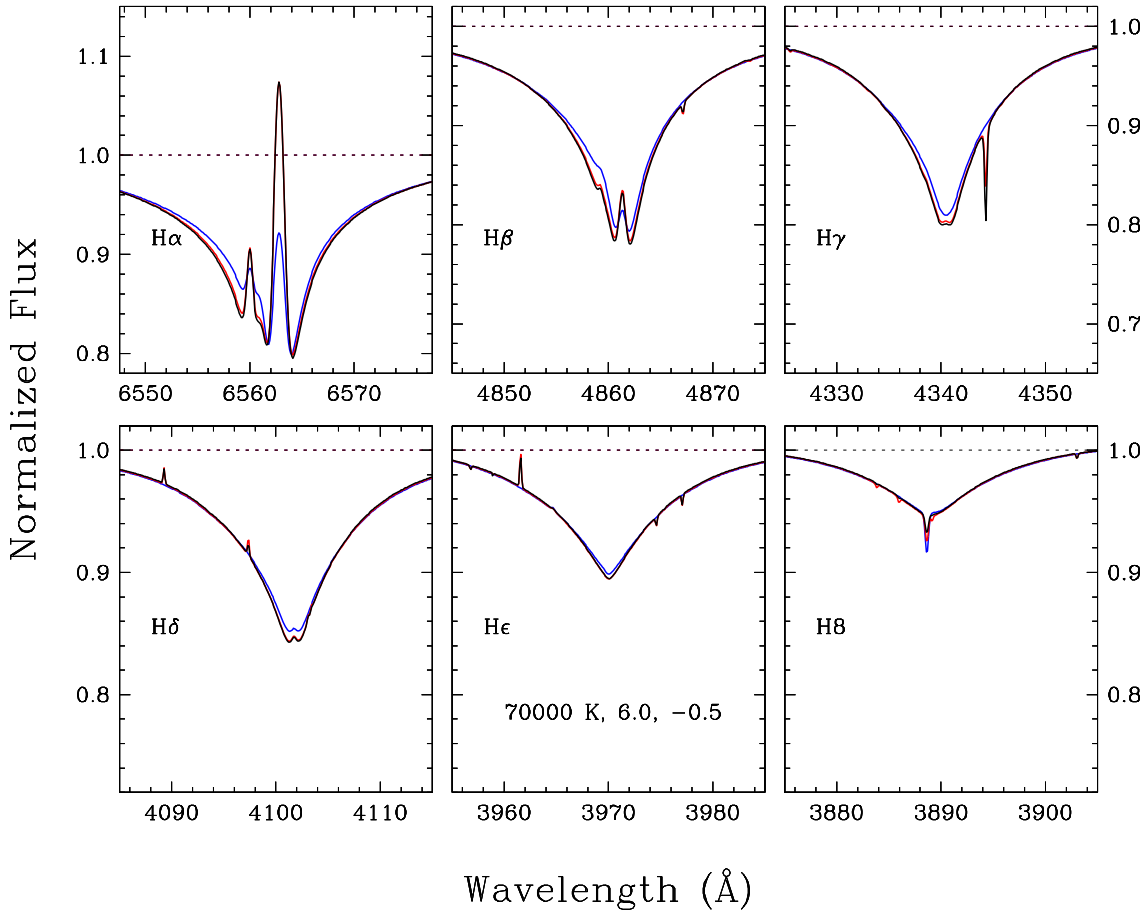

FIGURE 2.2 – (a) Comparison of the line profiles of the six lowest Balmer lines for a model with no metals (blue curves), a model with C, N, and O in solar abundances (red curves), and a model with C, N, O, and Fe in solar abundances (black curves). The models have otherwise the same parameters given by $T_{\rm eff}$ = 70,000 K, log g = 6.0, and log N(He)/N(H) = −0.5.

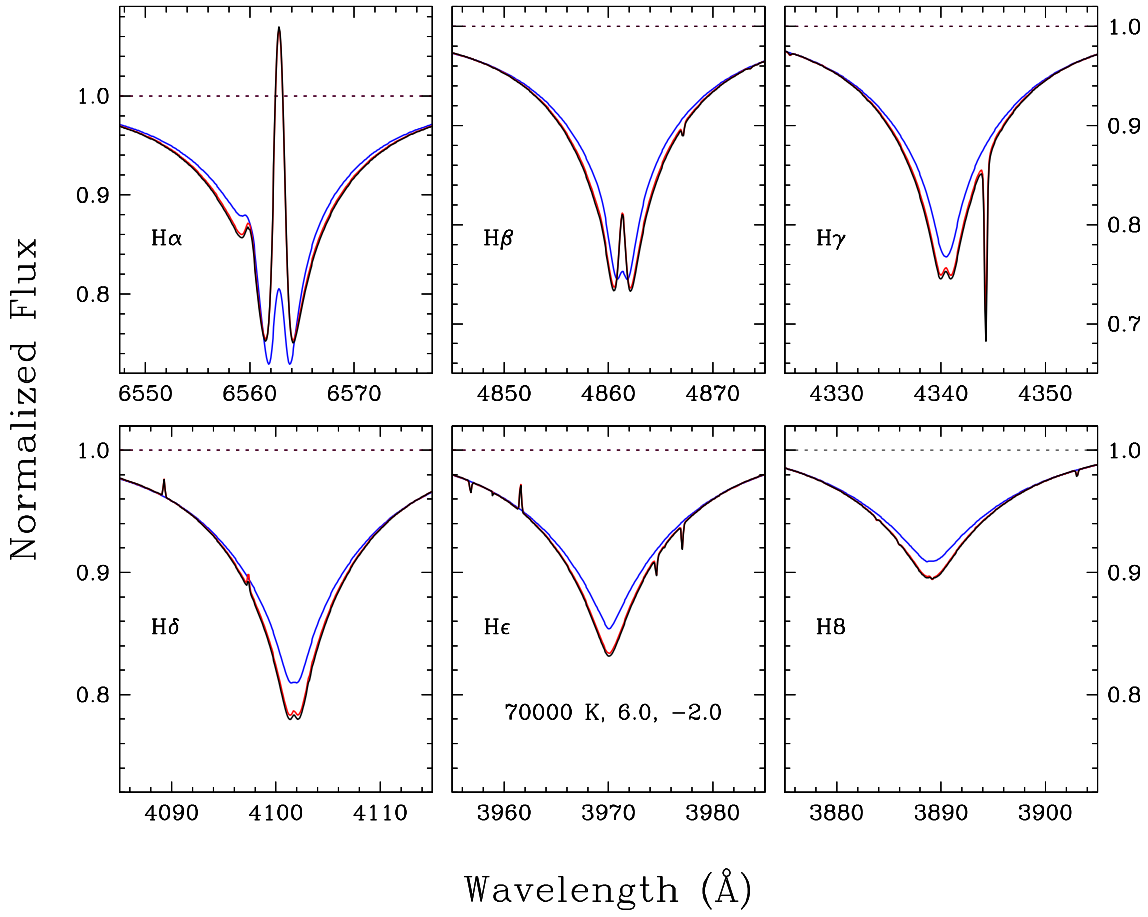

FIGURE 2.2 – (b) Similar to Fig. 2.2a, but for a helium abundance given by log $N(\mathrm{He})/N(\mathrm{H})$ = −2.0. A comparison with the previous figure clearly indicates that the helium abundance has a strong effect on the Balmer line profiles. One can also notice, in particular, the presence of an O IV (4344 Å) line in the red wing of Hγ.

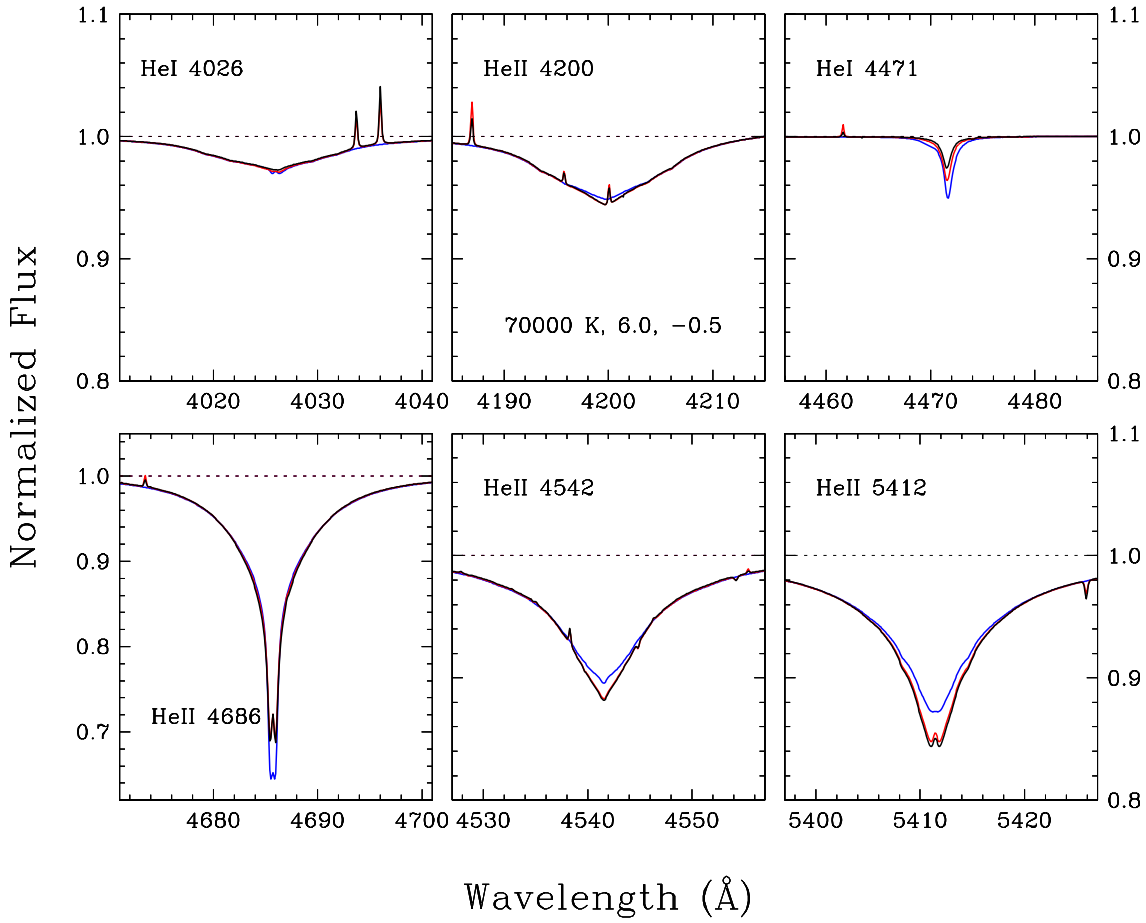

FIGURE 2.3 – (a) Similar to Fig. 2.2a, but for six important helium lines seen in the optical domain.

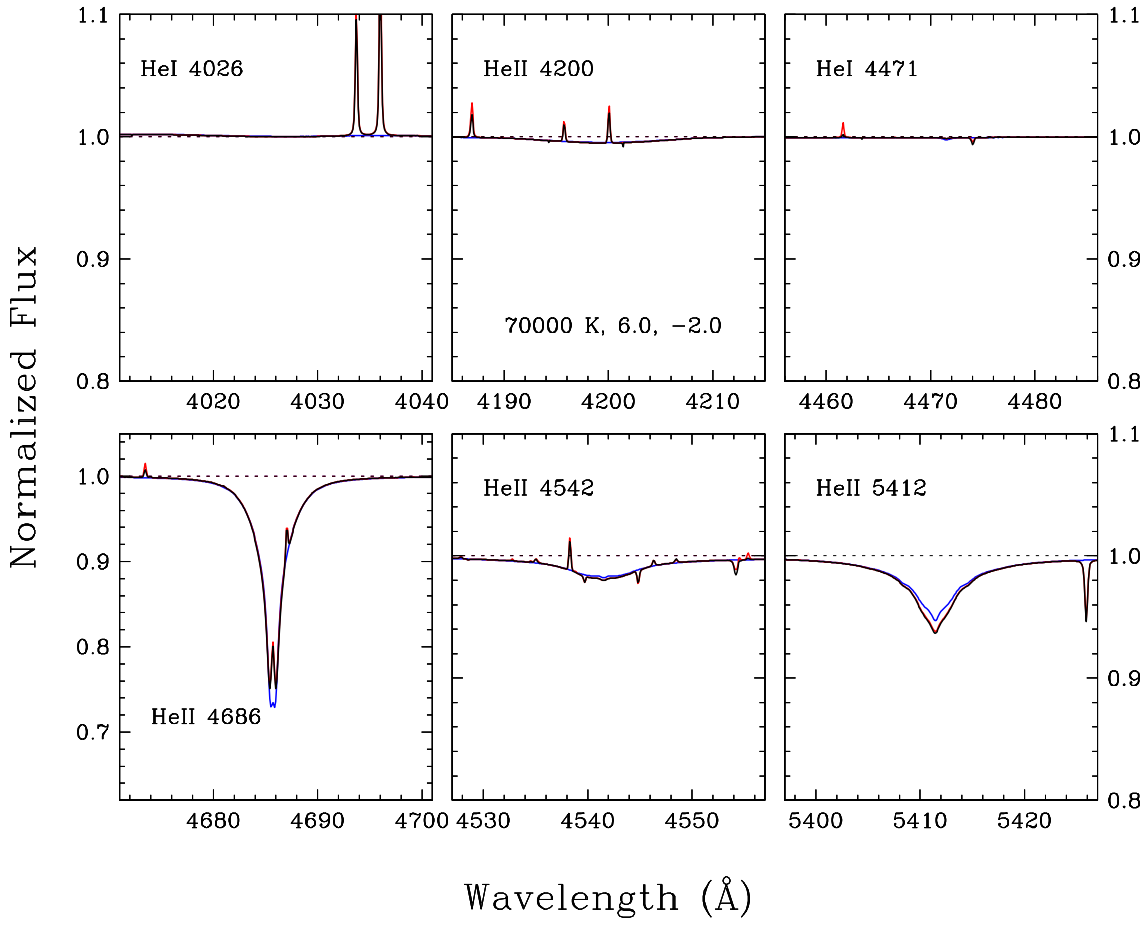

FIGURE 2.3 – (b) Similar to Fig. 2.3a, but for a helium abundance given by log N(He)/N(H) = −2.0. Two metal features in emission particularly stand up in the red wing of the very weak He I 4026 line. They are due to two O IV transitions at 4033.7 and 4036.0 Å.

in that it gives an indication of where in the atmosphere the various lines and the continuum are formed. For instance, one can infer from Figure 2.4 that the cores of lines such as Hα, Hβ, He II 4686, and He II 5412 in particular, are formed relatively high in the atmosphere and, therefore, are most sensitive to changes in the atmospheric structure that might occur in these layers due to a change in metallicity. This is in agreement with our observations above that the influence of metals is larger in these four lines, and that measurements of their profiles at high enough resolution would readily reveal their presence.

To conclude this subsection, we should mention the experiments reported by Haas et al. (1996) with model atmospheres at 90,000 K and $\log g = 6.0$, for which they found iron-group elements to cause significant changes in some H and He line profiles when the abundances of these metals are boosted to ten times their solar values. In our case, with the iron abundance only at its solar value, the effects of metal blanketing on the shapes of the hydrogen and helium lines are largely determined by the presence of C, N, and O. As can be observed in the previous figures, metal blanketing generally lead in our models to the broadening of the wings and deeper cores where, in some lines, central emission begins to appear. Qualitatively, these effects are the same as the ones noted by Haas et al. (1996). A glance at the populations of hydrogen and helium ions in our models shows that the inclusion of metals leads to a slight increase of singly-ionized helium in the region of line formation ($-2.0 \lesssim \log m \lesssim -1.0$), as well as in shallower layers. This behavior could be explained in part by the higher local temperature (see Figure 2.4), but since this increase in population is seen up to the surface, we can deduce that the main factor responsible for this overionization, and thus the more pronounced He II lines, is related to radiation coming from the deeper, hotter layers through NLTE transfer. As for neutral hydrogen, its population in line forming regions is not significantly affected by the presence of metals, but that population is nevertheless decreased in the outermost layers due, again, to overionization. Changes in hydrogen line profiles are therefore due mostly to different local and non-local conditions. In the case of the higher helium abundance, He II lines show larger changes than the Balmer lines, while for a subsolar abundance of helium the differences in the profiles of Balmer lines are enhanced.

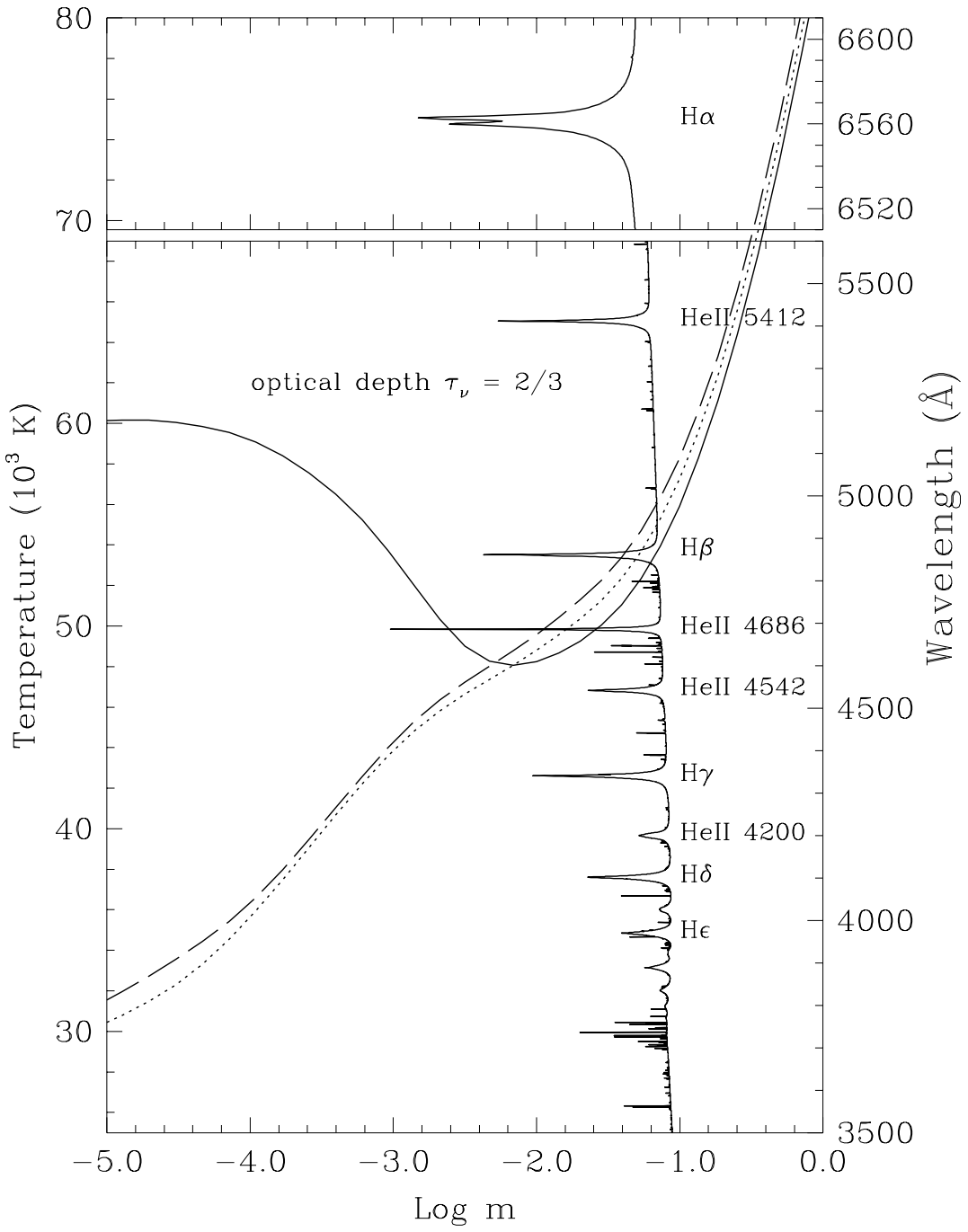

FIGURE 2.4 – Temperature stratification and monochromatic optical depth $\tau_\nu = 2/3$ as functions of depth, where m is the column density, for NLTE models defined by $T_{\rm eff}$ = 70,000 K, log g = 6.0, and log N(He)/N(H) = −0.5. The temperature structure is shown for models including H and He only (solid curve), H, He, and CNO in solar abundances (dotted curve), and H, He, and CNOFe in solar abundances (dashed curve). The $\tau_\nu = 2/3$ curve is shown for the model with the most metals.

2.3.4 NLTE and Line-Blanketing Effects on Derived Atmospheric Parameters

We have found it instructive to use our grids of model spectra in order to measure the importance of NLTE and metal line blanketing effects in a domain of the effective temperature-surface gravity plane that has remained relatively unexplored so far. Hence, in order to illustrate the effects due to departure from local thermodynamic equilibrium and metal line blanketing, we present a series of "maps" (Figures 2.5 to 2.7) basically constructed in the same way. All spectra from our grids were first degraded to a resolution of 9 Å in order to mimic observational data comparable to our Bok spectrum of J1600+0748. Some spectra from a chosen grid were then considered as "observed" data, and a fit on each of them was performed using another grid of theoretical models. The exact resolution used is not of importance in this type of exercise provided, of course, that both the "observed" and the theoretical spectra share the same resolution. The fits were done in order to find an optimal solution in terms of the effective temperature and the surface gravity, while the helium abundance was kept fixed during the procedure. In our maps, the dots represent the real values of log g and $T_{\rm eff}$ of the "observed" spectra, while the ends of each line segments give the results of the fitting procedure. We used the fitting technique described in Bergeron et al. (1992) – based on the numerical method of Levenberg-Marquardt (Press et al. 1986) – in order to perform simultaneous fits of the available hydrogen and helium lines. The uncertainties for those fits are typically between 10 and 50 K for $T_{\rm eff}$ and around 0.001 dex for log g.

Our first map, shown in Figure 2.5, illustrates the importance of NLTE calculations as inferred by analyzing "observed" spectra culled from the GHHe grid (NLTE H+He models) with theoretical spectra taken from the GHHeLTE grid (LTE H+He models). Results are presented for two values of the helium-to-hydrogen number ratio, log N(He)/N(H) = -0.5 and -2.5. It is easy to see that the use of LTE models in this range of parameters leads to huge underestimates of the effective temperature (reaching beyond 20,000 K in extreme cases) as well as large overestimates of the surface gravity (reaching up to 0.3 dex). We also point out from Figure 2.5 that a high helium abundance increases NLTE effects (the vectors get longer when log N(He)/N(H) increases at fixed $T_{\rm eff}$ and fixed log g), while a higher surface gravity

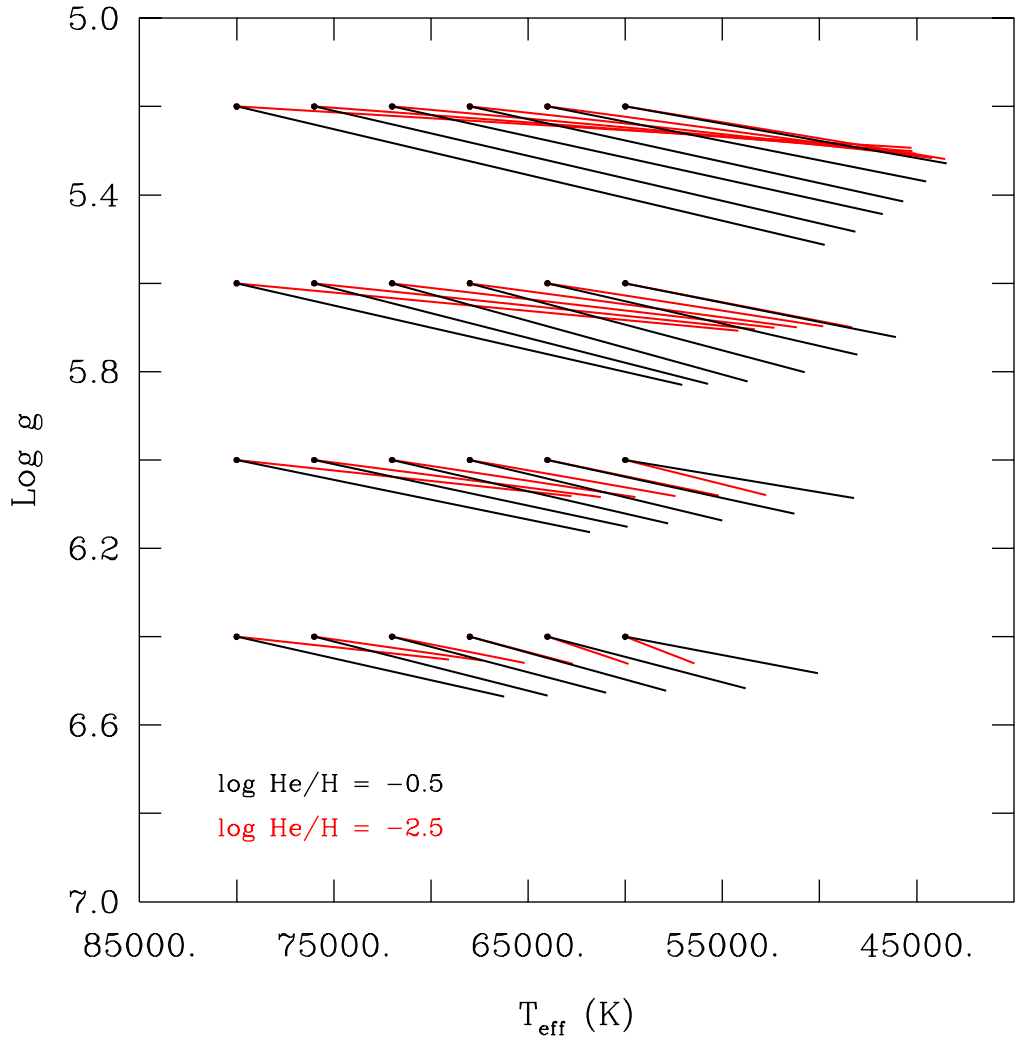

FIGURE 2.5 – Map illustrating NLTE effects on the inferred atmospheric parameters for models with no metals. The dots represent the exact values of log g and $T_{\rm eff}$ of NLTE models (GHHe), while the ends of line segments correspond to the parameters obtained when fitting those models with a grid of LTE synthetic spectra (GHHeLTE). Two different values of the helium abundance are considered : log N(He)/N(H) = −0.5 (black) and −2.5 (red).

tends to decrease them (the vectors get shorter when log g increases at fixed $T_{\rm eff}$ and fixed log N(He)/N(H)). We note in this connection that the NLTE effects uncovered here go in the same direction as those found by Liebert et al. (2005) and Napiwotzki et al. (1999) in models of hot DA white dwarfs for the surface gravity (i.e, our LTE sdO models overestimate log g as do their LTE DA models), but in the opposite direction for the effective temperature (i.e., our LTE sdO models underestimate $T_{\rm eff}$ contrary to their findings). This should cause no alarm because the LTE/NLTE vectors shown in Figure 3 of Liebert et al. (2005), for example, clearly rotate toward the "correct" effective temperature trend picked up in this study with decreasing log g, from the white dwarf range toward the hot subdwarf domain.

The line blanketing effects of metals on the inferred atmospheric parameters of representative models are next shown in Figures 2.6a and 2.6b. In the first case, the "observed" spectra were taken from the GHHeCNO grid (NLTE H+He+C+N+O models), and in the second case they were taken from the grid GHHeCNOFe (NLTE H+He+C+N+O+Fe models). Both sets were fitted with theoretical spectra belonging to the GHHe grid (NLTE H+He models). In addition, we considered three values of the helium-to-hydrogen number ratio in both plots, i.e., log N(He)/N(H) = -0.5 (black vectors), -1.5 (blue vectors), and -2.5 (red vectors). We find that, in the range of parameters surveyed, pure H+He models will tend to underestimate systematically the true surface gravity of sdO stars containing metals. On the other hand, the dependence on the effective temperature is not monotonic. For a star containing a low abundance of helium along with metals, an analysis based on models with no metals will lead to an underestimate of the true effective temperature by an amount that can be quite significant. For a star containing a relatively large abundance of helium, typified here by the case log N(He)/N(H) = -0.5, Figures 2.6a and 2.6b indicate that the true effective temperature can be either overestimated or underestimated, depending on the exact location of an object in the effective temperature-surface gravity plane. The same plots further illustrate the fact that the line blanketing effects due to metals tend to be less important in absolute terms when the helium content increases. This is in line with our remark above that the influence of metals on the line profiles of the H and He lines decreases with increasing He abundance.

The two maps shown in Figures 2.6a and 2.6b are rather similar, thus implying that the

principal effects of line blanketing are produced by the light metals (C, N, and O). To illustrate more clearly the small additional effects brought about by Fe, we present two other maps in Figures 2.7a and 2.7b, where we compare the blanketing vectors generated by fitting "observed" spectra from GHHeCNO (black line segments) and GHHeCNOFe (red line segments) with models with no metals (GHHe). The two plots refer to two different values of the helium-to-hydrogen ratio. It can be seen that the addition of Fe in solar abundance changes somewhat the inferred atmospheric parameters, but these changes are relatively small compared to the effects already produced by the presence of C, N, and O. This is particularly true in the case where the helium abundance is relatively low (Fig. 2.7b).

In our ranges of parameters, we can conclude that the effects of metal line blanketing on Balmer and helium lines are principally due to carbon, nitrogen, and oxygen. A similar conclusion was reached by Dreizler & Werner (1993) when they investigated the effects of C, N, O and iron-group line blanketing on the atmospheric structure of a model with $T_{\rm eff}$ = 90,000 K and log g = 6.0. Indeed, they found that the temperature structure of the outer layers to be only slightly different when they added iron-group elements (in solar proportions) to C, N, and O (also with solar abundances).

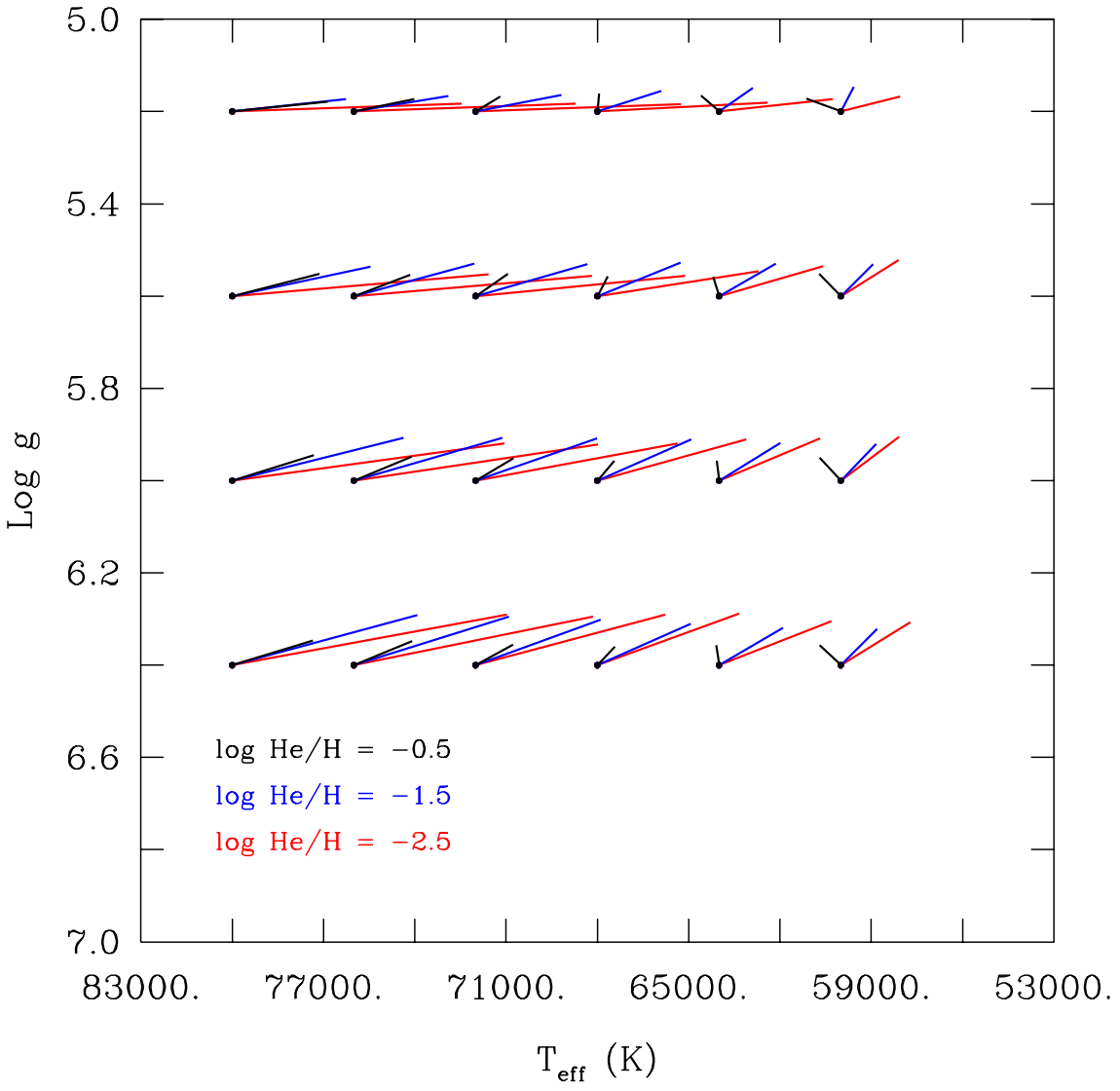

FIGURE 2.6 – (a) Map illustrating the effects of metal line blanketing on the inferred atmospheric parameters. Those parameters are obtained for models with C+N+O in solar abundances (GHHeCNO) using a grid of H+He models (GHHe). Three values of the helium abundance are considered : log N(He)/N(H) = −0.5 (black), −1.5 (blue), −2.5 (red).

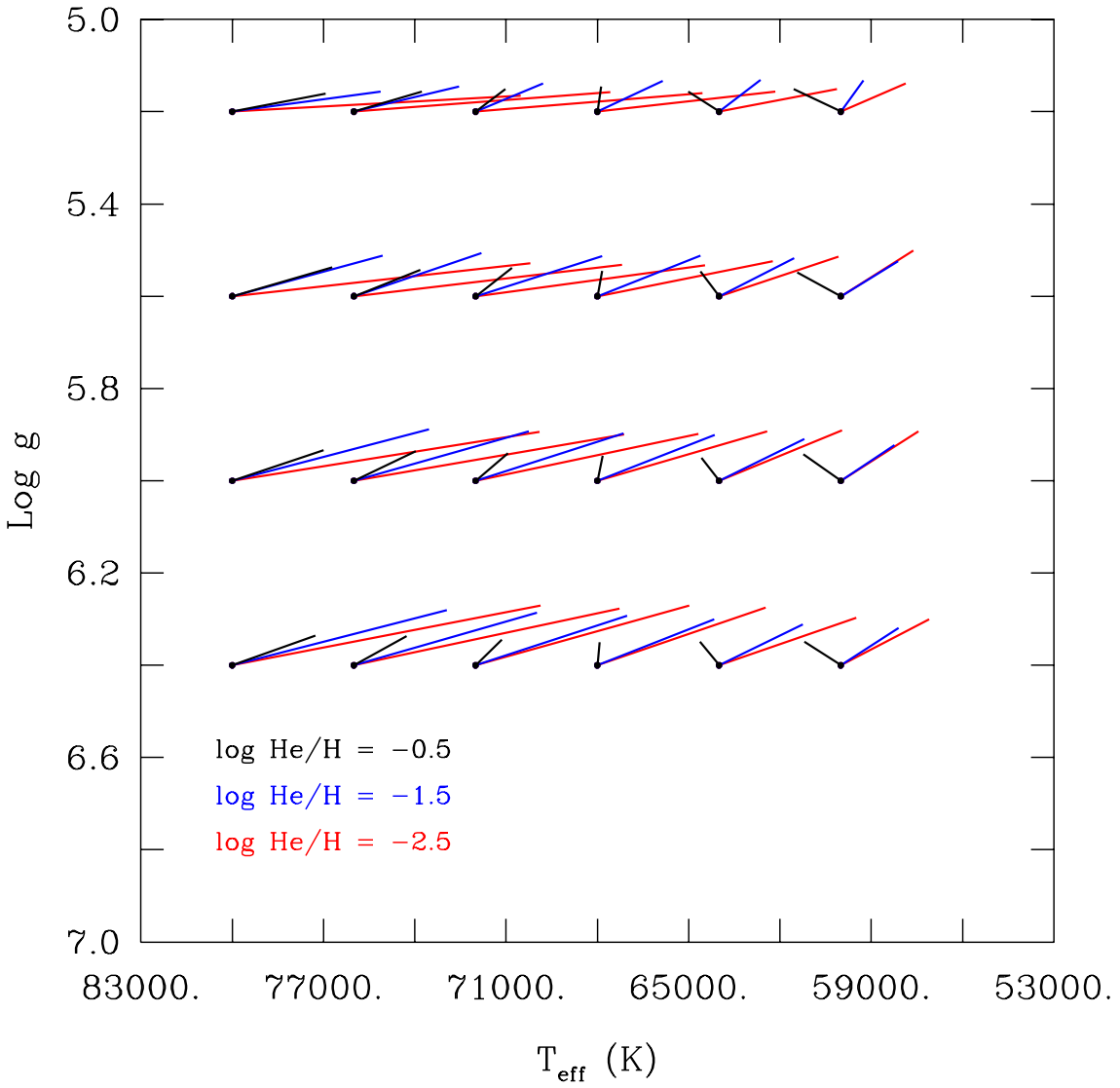

FIGURE 2.6 – (b) Similar to Fig. 2.6a, but for models including C+N+O+Fe in solar abundances (GHHeCNOFe) analyzed with a grid of H+He models (GHHe).

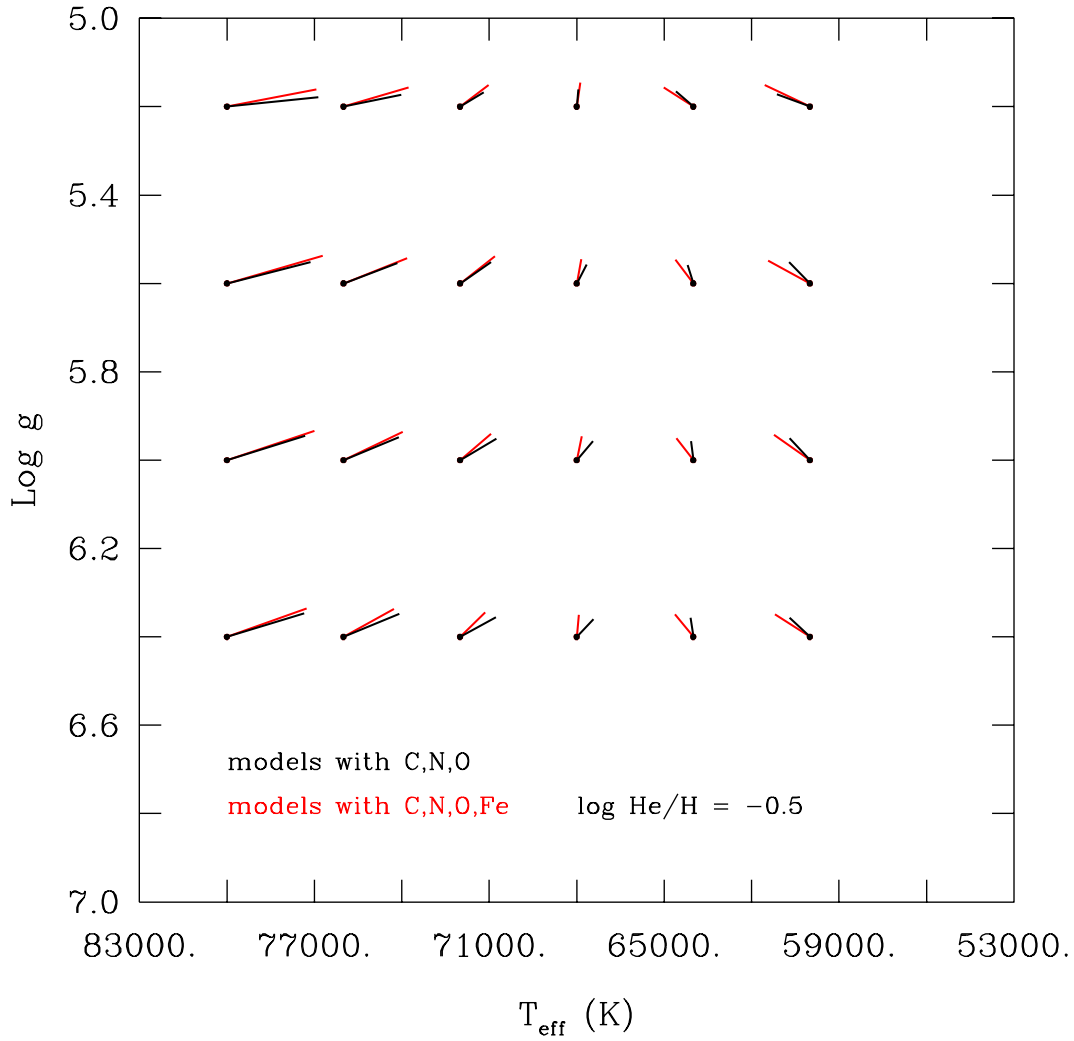

FIGURE 2.7 – (a) Results of the fitting procedure of some of our synthetic spectra with C+N+O (black vectors) and with C+N+O+Fe (red vectors) using our grid of models with H+He only. The helium abundance is fixed to a value log N(He)/N(H) = −0.5.

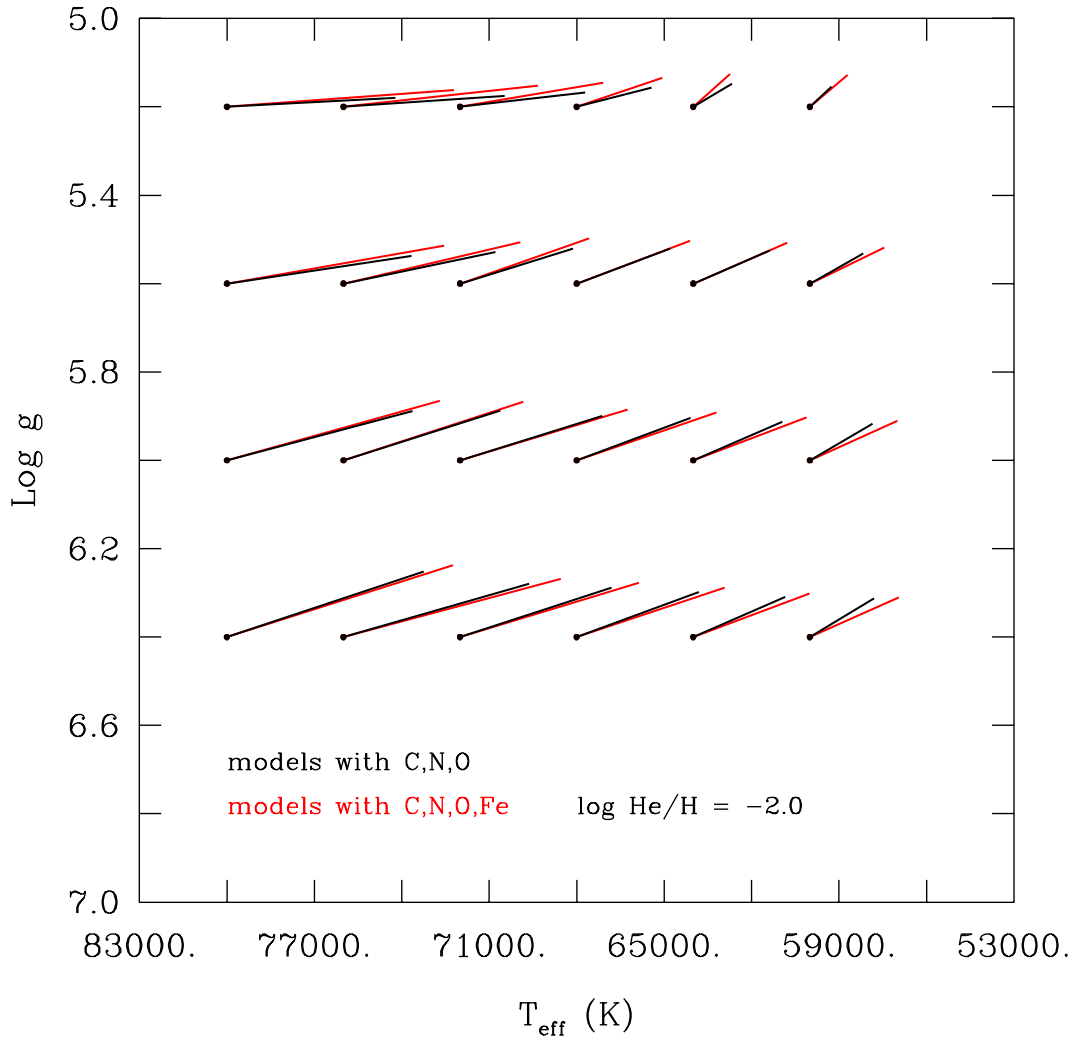

FIGURE 2.7 – (b) Similar to Fig. 2.7a, but for the case log N(He)/N(H) = −2.0.

2.4 Spectral Analysis of J1600+0748

2.4.1 Observational Material

Our spectral analysis of J1600+0748 is mostly based on a high-sensitivity (S/N∼180) optical spectrum of the system obtained at the Steward Observatory 2.3-m Bok Telescope with the B&C spectrograph. The total exposure time was 44,025 s, gathered over four nights (2007 March 28, May 07, 10, and 11). We used a 400 l $mm^{-}1$ 4889 Å grating in first order and a 2.5″ slit, covering the wavelength region 3620−6895 Å at 9 Å resolution. The spectra were wavelength calibrated using 48 non-blended He and Ar lines, and flux calibrated using the standard sdO stars Feige 34 and BD+28 4211, which were observed each night. The combined spectrum is shown by the top curve in Figure 2.8. The plot also illustrates the two flux-converted SDSS magnitudes of interest in this spectral range, namely, g = 17.41±0.01 and r = 17.62±0.01.

As first pointed out by Woudt et al. (2006), J1600+0748 is clearly a spectroscopic binary made of a hot sdO star and, most likely, a late-type main sequence companion. The spectrum shown in Figure 2.8 is indeed obviously "polluted" by the light of a cool star showing the Ca II K and H doublet at 3934−3968 Å , the G band around 4305 Å, and the Mg I complex at 5167−5184 Å as its most conspicuous features. We went to considerable lengths to determine the most probable spectral type of the companion, by cross-correlating the observed spectrum with numerous main sequence F, G, and K spectrum templates obtained with the same experimental setup. It is notable that the two best-matching G0V templates were superior even to F9 and G1 templates. We give details of our procedure in Appendix A.

The results of our efforts are shown by the middle curve of Figure 2.8 illustrating our cleansed spectrum, that of the sdO component. It is the result of the subtraction from the original spectrum (top curve) of the appropriately scaled and shifted average of the two G0V spectra (bottom curve). We note that the Bok spectrum of J1600+0748 was first presented in Fontaine et al. (2008). However, we have redone completely the reduction procedure in the meantime, with particular attention given to the flux calibration stage, a critical input in the cleansing procedure.

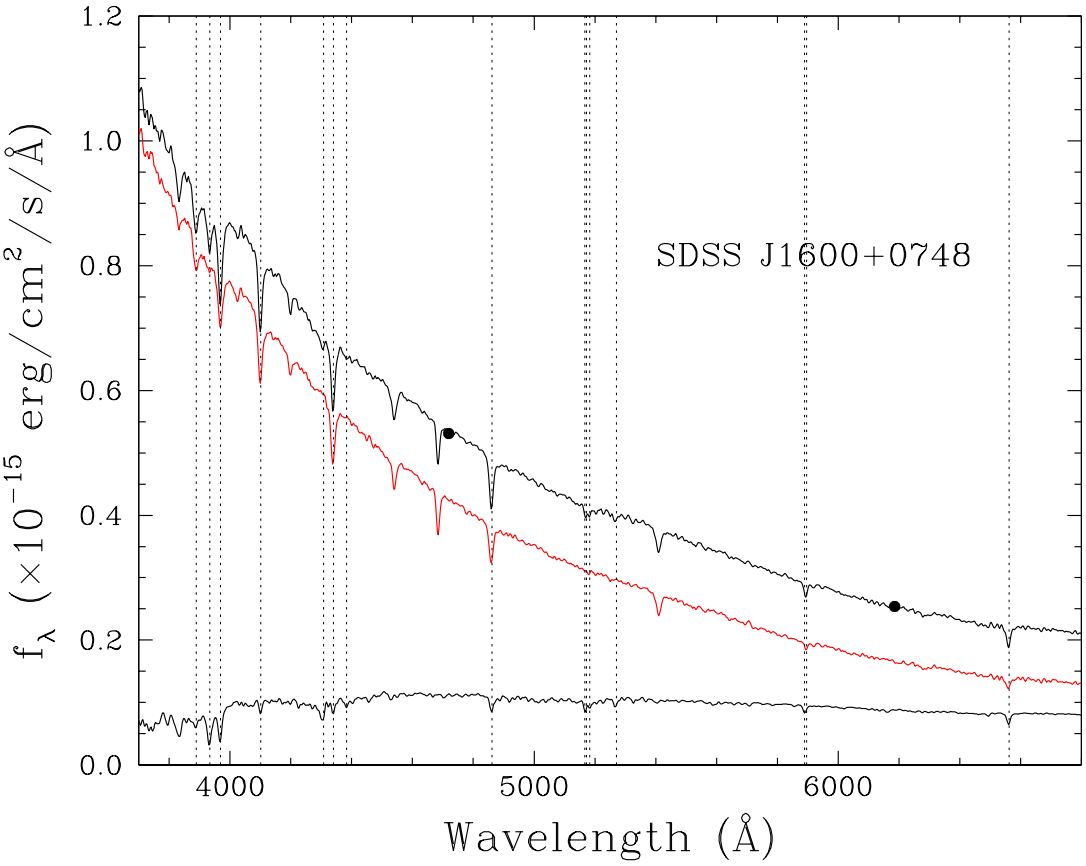

FIGURE 2.8 – Bok spectrum of the SDSS J1600+0748 system (top curve) ; template spectrum of the G0V companion (bottom curve) ; cleansed spectrum (middle curve, in red). Some conspicuous features (Fraunhofer lines) of the G0V star are indicated by vertical dotted lines. The two filled circles correspond to the SDSS magnitudes g and r.

The second spectrum comes from data that were kindly obtained for us by Jörg Dietrich during an unrelated observing run with EMMI at the New Technology Telescope (NTT) on La Silla, Chile, from May 7 to 10, 2007. After the main target had set, the last 1-2 hours of each night were dedicated to J1600+0748. We used Grating 4 and a slit width of $1''$ to yield spectra covering the $\sim$3500$-$5250 Å wavelength range with a resolution of $R = 840$ (or $\Delta\lambda \sim 5.2$ Å) at the central wavelength of 4350 Å. A total of 11 spectra with individual exposure times of 1200 or 1800 s were gathered, giving a combined exposure time of 16,920 s. The individual spectra were submitted to standard IRAF reduction routines, including bias and flat-field correction, flux extraction, sky subtraction and wavelength calibration, and were subsequently median combined. This resulted in a final spectrum with a S/N of $\sim$100 at the central wavelength. Unfortunately, this spectrum was not flux calibrated and we could not, therefore, attempt to cleanse it of the polluting light of the main sequence companion star.

Finally, we also considered the SDSS spectrogram of J1600+0748 available from the Sixth Data Release of the Sloan Digital Sky Survey (Adelman-McCarthy et al. 2008). The spectrogram can be retrieved with these parameters : Plate 1729, MJD 53858, Fiber 325, and has a resolution of $\sim$3 Å and a S/N$\sim$20 at Hβ. The SDSS spectrum is well flux calibrated, but it is very noisy and hardly suitable for a fitting technique that relies on a detailed comparison of the line profiles of H and He with those of model spectra, and not on the energy distribution. Because of that, we felt at the outset that the SDSS spectrum would likely not be suitable for our needs, and this is why we resolved to gather additional, higher sensitivity data.

Figure 2.9 illustrates the three spectra of the J1600+0748 system that we considered in this study. These data have not been cleansed of the polluting light of the companion. Given that the NTT spectrum is not flux calibrated, we carried out this comparison exercise with the normalized versions of the spectra. The flattening of the continuum has been done with the use of cubic spline functions. In practice, our line profile fitting technique boils down to using data similar to these normalized spectra because we define continuum points in both the observed data and model spectra (in exactly the same way), and we divide each spectral chunk of interest by the continuum defined by a straight line between two adjacent anchor points.

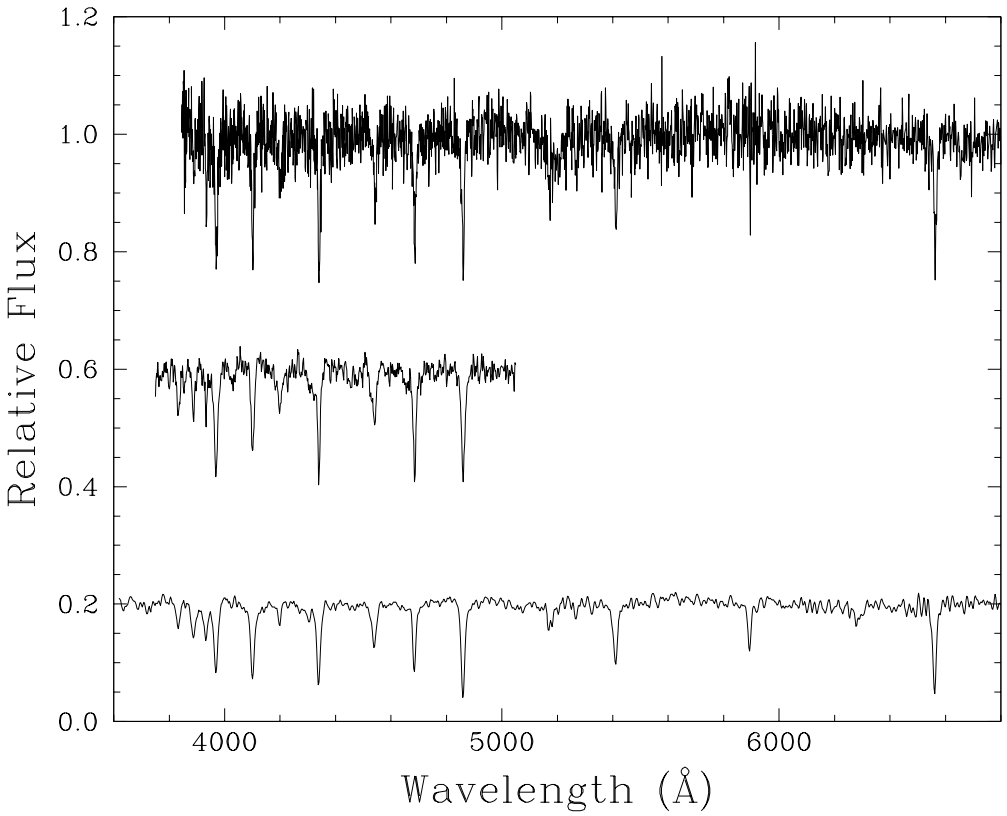

FIGURE 2.9 – Available normalized spectra of SDSS J1600+0748. From top to bottom : SDSS archive spectrum at 3 Å resolution, NTT spectrum at 5 Å resolution, and finally the Bok spectrum at a resolution of 9 Å on which relies most of our spectral analysis. Note that those three spectra are contaminated by the light of the main sequence companion.

To summarize, we considered in this study 1) a noisy polluted optical spectrum of the J1600+0748 system coming from the SDSS archives, 2) an intermediate sensitivity blue spectrum polluted by the light of the companion gathered at the NTT, 3) a high sensitivity polluted spectrum obtained at the Bok Telescope, and 4) a cleansed version of that spectrum showing mostly the light from the sdO component. Not surprisingly, as discussed in detail below, we obtained the most reliable spectral fits using the cleansed version of the Bok spectrum.

2.4.2 Derived Atmospheric Parameters

We analyzed the available spectra with the help of the five grids of models described in Table 2.1. Depending on the actual data (Bok, NTT, or SDSS), the theoretical spectra were degraded by convolution to the proper resolution corresponding to the experimental value prior to the fitting exercise. The latter was carried out in 3D space ($T_{\rm eff}$, log g, and log $N({\rm He})/N({\rm H})$) using a modified version of the minimization code originally written by our colleague Pierre Bergeron (see, e.g., Bergeron et al. 1992), to whom we are most grateful for making it available to us. This technique, which relies exclusively on the line profiles of H and He and not on the energy distribution, has the advantages that the results do not depend on interstellar reddening and are insensitive to small flux calibration errors.

Tables 2.2 and 2.3 summarize some of our results based on the Bok spectrum. Each line in these tables identifies the specific grid of models used in a fitting exercise as well as the type of input data analyzed (cleansed or polluted spectrum), and it lists the derived atmospheric parameters along with their formal fitting uncertainties. Because the S/N decreases significantly toward the red part of the spectrum due to our use of a blue-sensitive detector, and because the contribution of the main sequence companion becomes relatively more important toward the red also (see Figure 2.8), we realized that it would be useful to compare results obtained by fitting the whole spectrum with those derived by fitting only its blue part. Hence, Table 2.2 reports on derived atmospheric parameters obtained by fitting the data in the spectral range 3700−5600 Å, while Table 2.3 refers to fits using the full available range 3700−6800 Å. A comparison of the two tables indicates that adding the red part of the spectrum, which includes the weak He I lines at 5876 and 6678 Å along with Hα, only increases the formal

TABLE 2.2 – Results of our Fitting Procedure Using the Blue Part of the Bok Spectrum (3700−5600 Å)

Grid	$T_{\rm eff}$ (K)	log g (dex)	log N(He)/N(H) (dex)	Spectrum
GHHeLTE	57,107±2049	6.235±0.089	−0.820±0.059	cleansed
GHHe	68,595±1799	5.989±0.076	−0.640±0.051	cleansed
GHHeCNO	69,447±1742	6.070±0.072	−0.642±0.045	cleansed
GHHeCNOFe0.1	69,295±1734	6.075±0.072	−0.640±0.045	cleansed
GHHeCNOFe	68,500±1771	6.087±0.071	−0.636±0.045	cleansed
GHHeCNOFe	69,479±3387	5.880±0.114	−0.729±0.069	polluted

TABLE 2.3 – Results of our Fitting Procedure Using the Full Bok Spectrum (3700−5600 Å)

Grid	$T_{\rm eff}$ (K)	log g (dex)	log N(He)/N(H) (dex)	Spectrum
GHHeLTE	57,611±2579	6.301±0.112	−0.839±0.077	cleansed
GHHe	68,909±2439	6.020±0.103	−0.647±0.073	cleansed
GHHeCNO	68,684±2224	6.088±0.102	−0.651±0.067	cleansed
GHHeCNOFe0.1	68,559±2252	6.095±0.102	−0.649±0.067	cleansed
GHHeCNOFe	67,851±2346	6.109±0.101	−0.642±0.067	cleansed
GHHeCNOFe	68,047±2860	5.863±0.111	−0.747±0.071	polluted

uncertainties on the inferred atmospheric parameters, while the latter remain fully consistent with those found on the basis of the blue part of the spectrum. In the following, we therefore concentrate on the most reliable results, as summarized in Table 2.2.

Our analysis of the blue part of the cleansed Bok spectrum leads to inferred parameters for the sdO component of J1600+0748 that cannot be formally distinguished on the basis of any of the four NLTE model grids that we used. Indeed, Table 2.2 reveals that the derived parameters are nearly the same, whatever the grid considered (GHHe, GHHeCNO, GHHeCNOFe0.1, or GHHeCNOFe), thus indicating that metal line blanketing effects in J1600+0748 are likely not very important. Nevertheless, we do get qualitatively better fits to the H and He line profiles with increasing metallicity. We point out that this qualitative improvement is not necessarily reflected in the values of the formal uncertainties quoted in Table 2.2. This is because the numerous metal lines, present in various quantities from one model grid to another, produce as many small wiggles in the theoretical spectra when those are degraded to a resolution of 9 Å

to match that of the data. In that case, the numerous mismatches between this fine structure and the actual spectrum (that may or may not contain the metals in the assumed quantities) contribute to the formal uncertainties. In other words, the formal uncertainties on the derived parameters provide primarily a quantitative estimate of the quality of a fit to the H and He line profiles, but, by construction here, they also include some "noise" associated with the presence of metal lines in the models.

Figures 2.10a and 2.10b illustrate perfectly the qualitative improvement that we find with increasing metallicity. The former shows our model fit (heavy curve) to all the hydrogen and helium lines (thin curve) available in the blue part of our cleansed Bok spectrum of J1600+0748 using a model grid (GHHe) with no metals. The latter shows the corresponding fit, the best that we have achieved, using our grid with the most metals (GHHeCNOFe). Even though the changes can only be small (as expected in view of the numbers listed in Table 2.2), one can still easily notice real improvements in going from Figure 2.10a to Figure 2.10b for several fitted H lines, particularly Hβ, Hγ, H8, and H9. Likewise, a significant improvement is observed for the fit to the profile of the He II 5412 Å line, and, to a lesser extent, for that of the He II 4542 Å feature as well. In fact, the overall simultaneous fit to all available H and He lines shown in Figure 2.10b is quite good by any standards. Nevertheless, we cannot fail but notice that the predicted strengths of the He II features at 4542, 4686, and 5412 Å are still somewhat too low compared to the data, which suggests to us that some additional metal line blanketing might be needed for further improvement.

Another point of interest concerning Figures 2.10a and 2.10b is the suggestion of the possible detection of an O IV feature at 4632 Å. We recall that this line is the strongest metal feature that is present in our synthetic spectra in the ranges of effective temperature, surface gravity, and helium-to-hydrogen number ratio of interest for the sdO component in the J1600+0748 system (see Figure 2.1 above). We note, from Figure 2.10b, that the observed "feature" near 4632 Å is rather well reproduced by our theoretical profile corresponding to a solar amount of oxygen. While we find this result rather interesting and suggestive, caution is nevertheless advised here because we cannot be certain at this stage if this feature is real or caused by some residual effect of the cleansing procedure.

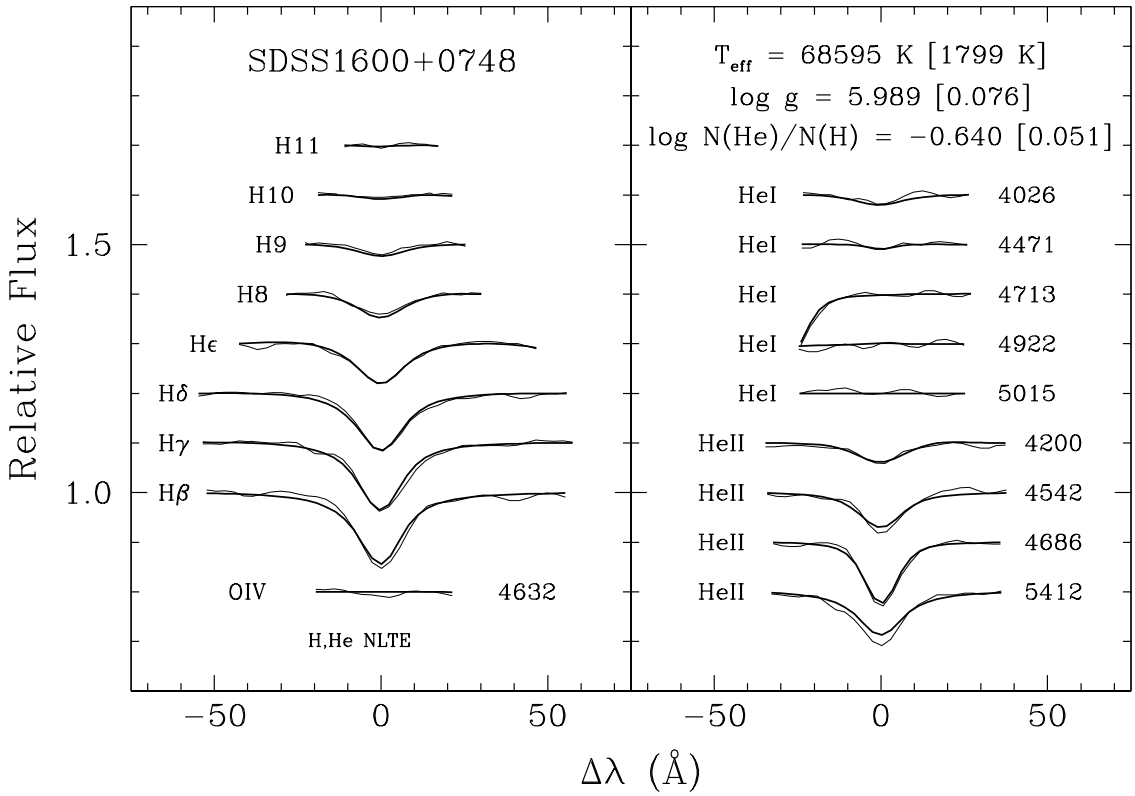

FIGURE 2.10 – (a) Best fit to the blue part (wavelengths < 5500 Å) of the cleansed Bok spectrum of SDSS J1600+0748 using H+He NLTE models (3D grid GHHe).

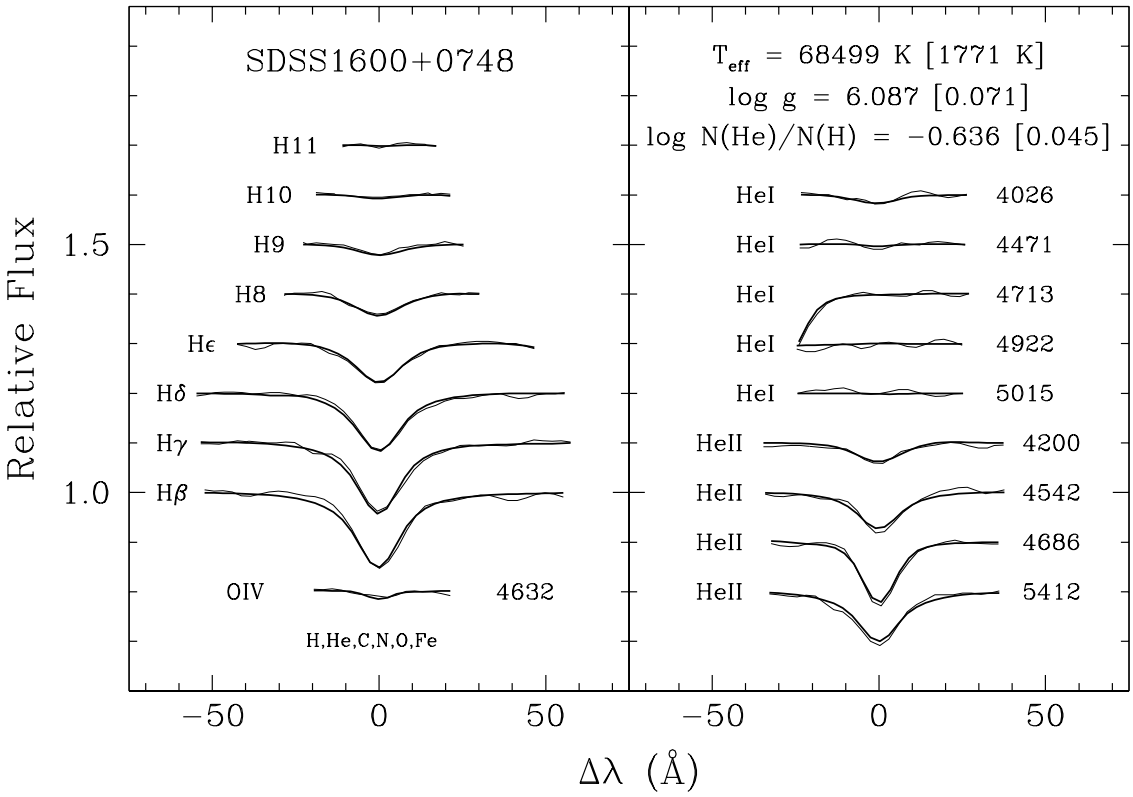

FIGURE 2.10 – (b) Similar to Fig. 2.10a, but using our 3D grid of NLTE model spectra containing C, N, O, and Fe in solar abundances (GHHeCNOFe). Compared to the case depicted in Fig. 2.10a, slight but real improvements can be detected in several fitted Balmer line profiles, notably for Hβ, Hγ, H8, and H9. Likewise, a noticeable improvement is achieved for the He II 5412 Å feature, and, to a lesser extent, for the 4542 Å line as well. Note also the small bump around 4632 Å in the observed spectrum that is rather well reproduced by an O IV line.

Our finding that metal line blanketing effects in the atmosphere of J1600+0748 are not very large, although certainly present, can be explained by the fact that, by accident, that sdO star finds itself in a region of parameter space where such effects do not leave strong signatures on the H and He line profiles. In particular, as discussed above in §2.4, the relatively high helium abundance ($\log N(\mathrm{He})/N(\mathrm{H}) \simeq -0.64$) found in its atmosphere contributes most importantly to reduce these effects. To understand this better, let us consider two model spectra with parameters similar to those inferred for J1600+0748 in Table 2.2. Specifically, we pick two models defined both by $T_{\rm eff}$ = 68,000 K, $\log g = 6.0$, and $\log N(\mathrm{He})/N(\mathrm{H}) = -0.5$, but one from the GHHe grid (no metals) and the other from the GHHeCNOFe grid (full metals). The maps shown in Figure 2.6b and Figure 2.7a then clearly reveal that the line blanketing vector associated with those two models is quite small for the chosen helium abundance, and, furthermore, that it is almost vertical, meaning that the effects on the effective temperature are almost negligible. The vector predicts only a small reduction of the value of the surface gravity when metal blanketing effects are totally neglected under those conditions. This agrees qualitatively very well with the numbers listed in Table 2.2 for the parameters inferred on the basis of the GHHe grid compared to those inferred using the GHHeCNOFe grid.

It should be pointed out that the relative insensitivity of the inferred atmospheric parameters of the J1600+0748 sdO component on the presence of metals is a very good thing from the point of view of the exploratory pulsational survey carried out by Fontaine et al. (2008). Those authors have proposed, among other things, a plausible seismic model for J1600+0748 which requires, however, values of the effective temperature and surface gravity similar to those found here [7]. That model could have been jeopardized, had we found atmospheric parameters highly dependent of the unknown metallicity. Since this is not the case, we feel confident that the parameters defining the atmosphere of J1600+0748 are now relatively well secured, and that the pulsational calculations of Fontaine et al. (2008) rest on solid grounds.

We have also investigated the consequences of using the original, polluted version of the Bok spectrum in order to evaluate the criticalness of our cleansing operation described above.

7. The atmospheric parameters inferred in Fontaine et al. (2008) are consistent with those given in Table 2.2. They are based on an analysis of the blue part of the Bok spectrum – which we rereduced in the meantime – using an older NLTE H+He model grid.

TABLE 2.4 – Results of our Fitting Procedure Using the Available Polluted Spectra

Grid	$T_{\rm eff}$ (K)	log g (dex)	log N(He)/N(H) (dex)	Spectrum
GHHeCNOFe	68,047±2860	5.863±0.111	−0.747±0.071	Bok
GHHeCNOFe	65,298±3529	5.643±0.146	−0.576±0.101	NTT
GHHeCNOFe	63,546±3700	5.511±0.165	−0.668±0.125	SDSS

We report the results of our fitting procedures using the GHHeCNOFe grid on the last line of both Table 2.2 and Table 2.3. Perhaps surprisingly, we find that the inferred parameters are not drastically different from their counterparts obtained from the cleansed version of the spectrum (next-to-last line in the tables). Even though there are clear trends (the derived effective temperature is higher, the surface gravity is lower, and the helium abundance is lower when using the polluted data), the values of the parameters overlap when due account of the uncertainties is taken. We conclude from these experiments that, while highly desirable, the cleansing operation is not absolutely critical for the determination of the atmospheric parameters. In particular, the precise nature of the cool companion star is not a fundamental issue in the process.

To be complete, we included in both Table 2.2 and Table 2.3 the results of our fitting technique using the grid of LTE H+He model spectra. These results are reported on the first line and should be compared with those listed on the second line. One can see that the LTE approximation in these ranges of parameters leads to a drastic underestimate of the true effective temperature and, likewise, a relatively large overestimate of the surface gravity. These effects can be directly related to the map depicted in Figure 2.5 above.

Finally, we present the results of some of our fitting exercises using the other spectra that we have available on J1600+0748. Because the NTT spectrum is not flux calibrated, we could only analyze it in its polluted form. Since we want to compare things that are comparable, we have therefore retained the polluted version of the Bok spectrum and the original SDSS spectrum. Table 2.4 summarizes our results in the cases where the GHHeCNOFe grid has been used. Because the S/N decreases as one reads down in Table 2.4, the fitting errors on the derived parameters increase accordingly. However, we find some intriguing trends : both

the estimated effective temperature and surface gravity decrease when going from the Bok, to the NTT, to the SDSS spectrum. While the three different estimates of $T_{\rm eff}$ remain formally consistent, this is not the case for $\log g$. We do not know why this is so, but, in any case, these results do not appear very reliable to us.

The situation is well depicted in the series of plots (Figs. 2.11a, 2.11b, and 2.11c) showing, on the exact same scale, the details of the fits obtained using these three spectra. Note the obvious pollution due to the Ca II H and K lines affecting the Hϵ spectral region in each of these spectra. Clearly here, the S/N makes the difference, to the point where the SDSS spectrum is nearly useless in this approach where the line profiles are fitted and the energy distribution is ignored. We suggest, in this context, that the muti-parameter approach used by Rodríguez-López et al. (2010) to analyze the SDSS spectrum of J1600+0748, and which is based mostly on the energy distribution, is no doubt reliable for estimating the effective temperature of the sdO component but, at the same time, much less so for pinning down the surface gravity. Indeed, the energy distribution of a hot sdO star in the optical domain is quite insensitive to the surface gravity, meaning that the latter parameter can only be reliably determined through line profile fitting. However, as we have just seen in Figure 2.11c, the SDSS spectrum of J1600+0748 is much too noisy for that task. We believe, on this basis, that the low value of $\log g = 5.25\pm0.30$ proposed by Rodríguez-López et al. (2010) is quite uncertain. Otherwise, their other estimates of $T_{\rm eff} = 70{,}000\pm5000$ K and $\log N({\rm He})/N({\rm H}) = -0.51\pm0.16$ for that star are perfectly consistent with our best values given in Table 2.2.

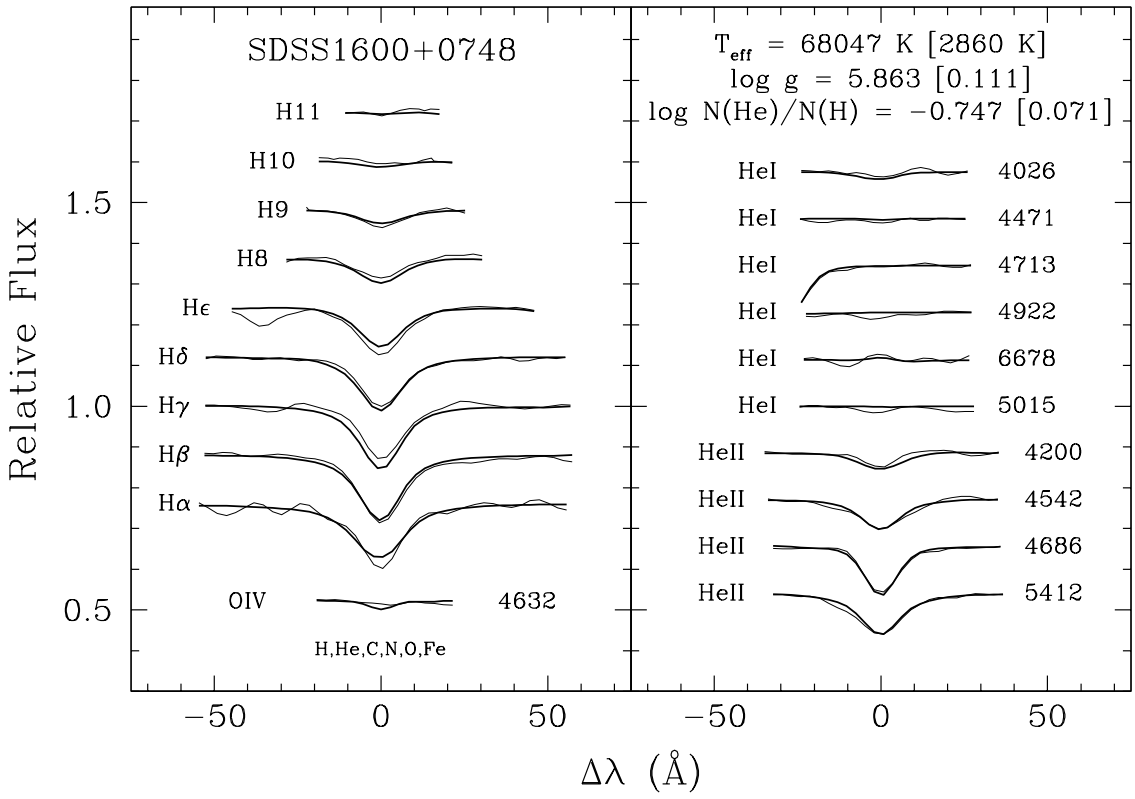

FIGURE 2.11 – (a) Best fit obtained for the full, but polluted, Bok spectrum using our 3D NLTE model grid with C+N+O+Fe in solar abundances (GHHeCNOFe).

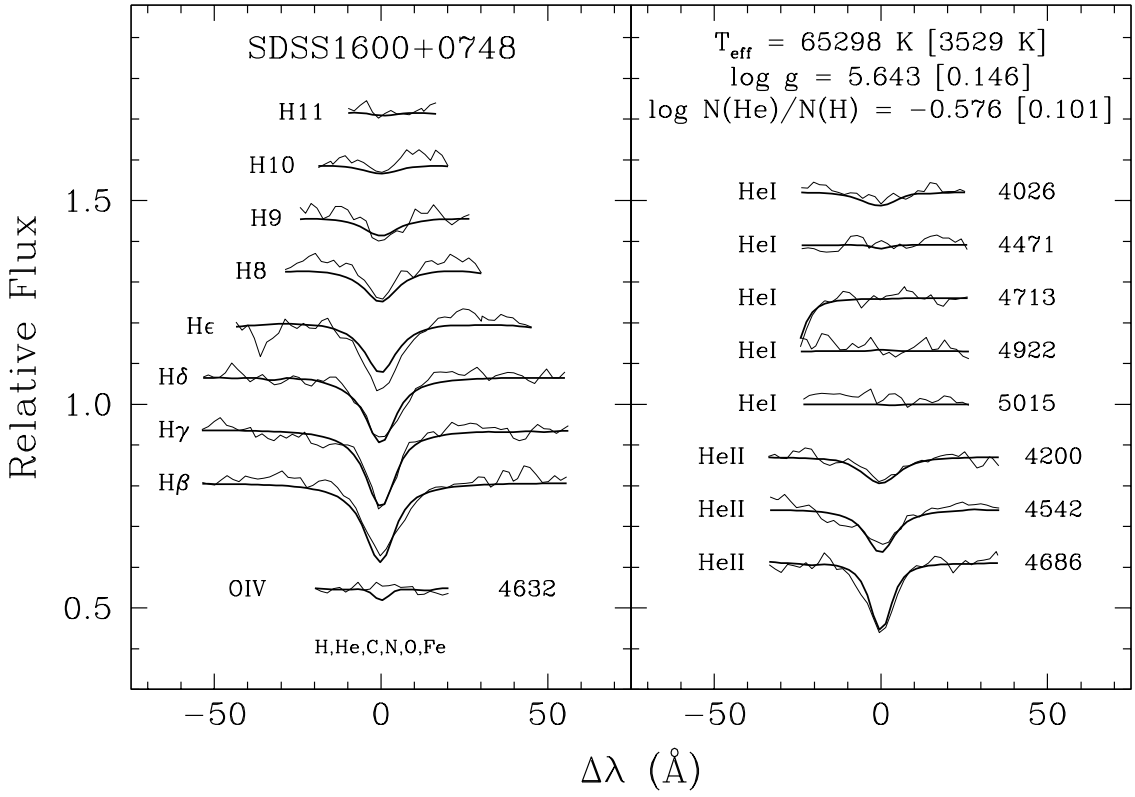

FIGURE 2.11 – (b) Similar to Fig. 2.11a, but for the full (polluted) NTT spectrum.

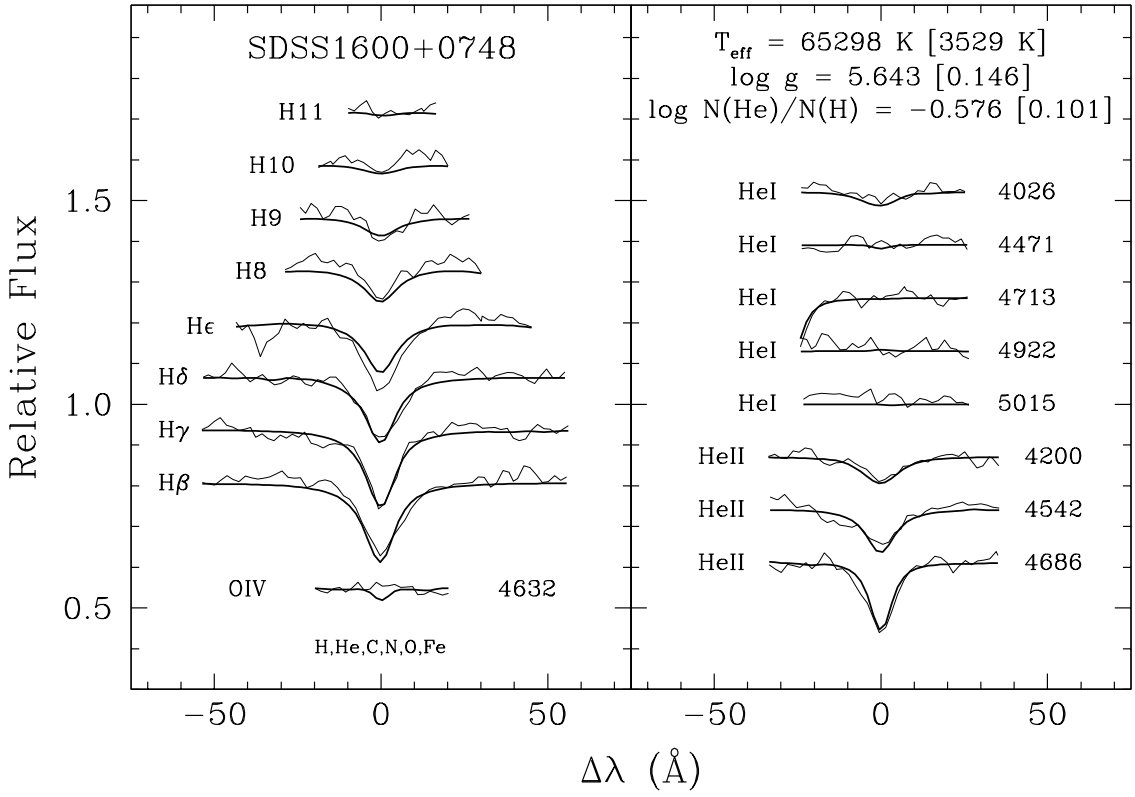

FIGURE 2.11 – (c) Similar to Fig. 2.11a, but for the full (polluted) SDSS spectrum.

2.5 Conclusion

We have carried out a detailed analysis of the optical spectrum of the J1600+0748 system, which is an unresolved pair made of a hot sdO star and of a much cooler companion, probably a main sequence star. The interest in this system stems from the fact that the sdO component currently defines by itself the class of pulsating hot subdwarf O stars (Woudt et al. 2006). As such, it is important to characterize as well as possible this unique star and, in particular, to locate with precision its location in the effective temperature-surface gravity plane. This is essential for constraining eventual detailed seismic models of this star in a previously unexplored instability region of the HR diagram.

Prior to this work, there have been two independent analyses based on optical spectroscopy aimed at estimating the atmospheric parameters of the pulsating sdO component in the J1600+0748 system (Fontaine et al. 2008 and Rodríguez-López et al. 2010). Both these studies relied on sophisticated NLTE model atmospheres and spectra as appropriate for such a hot star, but they were limited by the fact that the only elements included in the calculations were hydrogen and helium, and no heavier elements. We therefore sought to investigate the effects of metallicity on the derived atmospheric parameters. Although the tools to carry out that task properly – the public codes TLUSTY and SYNSPEC, for example – have been available for a while, there remained the formidable technical problem of being able to compute large grids of NLTE model atmosphere and spectra over a practical period of time when taking into account metals, particular iron-peak elements. We got around that problem through the use of CALYS, a dedicated small cluster of PC's (80 processors), on which TLUSTY and SYNSPEC were adapted to run in parallel mode. With the use of CALYS, it still took us several weeks of CPU time to complete the five grid of models described in Table 2.1.

We first took advantage of the availability of these grids to investigate the effects of metal line blanketing on the theoretical optical spectra in a regime that had not been explored in detail before (60,000 K $\leq T_{\rm eff} \leq$ 80,000 K ; 4.8 $\leq \log g \leq$ 6.4 ; $-4.0 \leq \log N({\rm He})/N({\rm H}) \leq$ 0.0). We found that the neglect of metal blanketing leads to systematic underestimates of the surface gravity in the ranges covered by our grids. On the other hand, the effective temperature may be either underestimated or overestimated, depending on the specific conditions. We also

discovered that the helium-to-hydrogen ratio influences quite importantly the impact of metal blanketing on the resulting spectra. Indeed, a low helium abundance ($\log N(\mathrm{He})/N(\mathrm{H}) \lesssim -1.5$) allows metal blanketing to leave relatively large signatures on the H and He line profiles, while a high helium abundance tends to mask such effects. We also found that the addition of Fe (solar abundance) leads only to small incremental effects on the atmospheric structure and, consequently, on the model line profiles of H and He as compared to the case where the metallicity is defined by C+N+O (solar abundances).

With the help of these model grids, we next analyzed the three data sets that were available to us on J1600+0748. Two of these consisted of optical spectra that we respectively obtained at the Bok Telescope in Arizona and at the NTT in Chile. The third one is the optical spectrum of J1600+0748 that we retrieved from the SDSS archives. It quickly became apparent, however, that the much superior sensitivity of our Bok spectrum (S/N$\sim$180) compared to that of the other two observed spectra would supersede any other considerations (such as a reduced resolution) in terms of obtaining the most reliable atmospheric parameters. In practice, therefore, our most significant results were all based on the Bok spectrum.

One difficulty that we had to face concerning the optical spectrum of J1600+0748 is how to handle the pollution caused by the presence of the unresolved main sequence companion. We invested special efforts to identify as best we could the nature of that companion and, in the end, we concluded that it is likely a G0V star. We were thus able to produce a "cleansed" spectrum for the pulsating sdO component of the system as illustrated by the middle curve in Figure 2.8. In a comforting experiment (see the numbers reported in Tables 2.2 and 2.3), we compared the results of fitting the cleansed spectrum with those obtained when we used the original polluted spectrum, and we found out that the inferred parameters are not significantly different given the uncertainties. This implies that the exact nature of the companion is not a critical issue in terms of characterizing properly the atmospheric properties of the sdO component.

Our best and most reliable result is based on the fit to the blue part of the Bok spectrum achieved with NLTE synthetic spectra that include C, N, O, and Fe in solar abundances, leading to the following parameters for the pulsating sdO star in J1600+0748 : $T_{\mathrm{eff}} = 68{,}500$

$\pm$ 1770 K, log g = 6.09 $\pm$ 0.07, and log N(He)/N(H) = $-$0.64 $\pm$ 0.05 (formal fitting errors only). Figure 2.10b illustrates the details of that very good fit to the available H and He lines. This combination of parameters, particularly the relatively high value of the helium abundance, implies that line blanketing effects due to metals are not very large in the atmosphere of this sdO star. And indeed, Table 2.2 provides ample evidence of this. We thus conclude that our derived atmospheric parameters for the J1600+0748 sdO component are relatively secure, even though the true metallicity is still unknown. These happy circumstances strengthen the case for the seismic model put forward by Fontaine et al. (2008) on this interesting star. Nevertheless, it would be valuable in the future to refine the characterization of J1600+0748 by actually carrying out a detailed abundance analysis of the metals that must be present in the atmosphere of the sdO component. This would be best be done using the COS instrument onboard *HST*.

We are most grateful to Ivan Hubeny and Thierry Lanz for having developed, maintained, and made publicly available the powerful tools that are TLUSTY and SYNSPEC. This work was supported in part by the NSERC of Canada. G.F. also acknowledges the contribution of the Canada Research Chair Program. Some of the observations reported here were collected at the European Organisation for Astronomical Research in the Southern Hemisphere, Chile (proposal ID 079.A-0369).

Bibliographie

Adelman-McCarthy, K. et al. 2008, ApJS, 175, 297

Bergeron, P., Saffer, R.A., & Liebert, J. 1992, ApJ, 394, 228

Blanchette, J.-P., Chayer, P., Wesemael, F., Fontaine, G., Fontaine, M., Dupuis, J., Kruk, J. W. & Green, E. M. 2008, ApJ, 678, 1329

Deetjen, J. L. 2000, A&A, 360, 281

Dreizler, S. & Werner, K. 1993, A&A, 278, 199

Fontaine, G., & Brassard, P. 2008, PASP, 120, 1043

Fontaine, G., Brassard, P., Green, E. M., Chayer, P., Charpinet, S., Andersen, M., & Portouw, J. 2008, A&A, 486, L39

Gianninas, A., Bergeron, P., Dupuis, J., & Ruiz, M.T. 2010, ApJ, 720, 581

Grevesse, N. & Sauval, A. 1998, Space Sci. Rev., 85, 161

Haas, S., Dreizler, S., Heber, U., Jeffery, S. & Werner, K. 1997, A&A, 311, 669

Hubeny, I. 1988, Comput. Phys. Commun., 52, 103

Hubeny, I. & Lanz, T. 1995, ApJ, 439, 875

Kurucz, R. L. 1988, in IAU Trans., ed. M. McNally, Vol. 20B (Kluwer : Dordrecht), 168

Lanz, T. & Hubeny, I. 2007, ApJS, 169, 38

Lanz, T. & Hubeny, I. 2003, ApJS, 146, 417

Lanz, T., Hubeny, I. & Heap, S. R. 1997, ApJ, 485, 843

Latour, M., Fontaine, G., Brassard, P., Chayer, P. & Green, E. M. 2010 Ap&SS, published online 03/2010

Liebert, J., Bergeron, P. & Holberg, J. B. 2005, ApJS, 156, 47

Napiwotzki, R., Green, P. J., Saffer, R. A. 1999, ApJ, 519, 399

Press, W. H., Flannery, B. P., Teukolsky, S. A., & Vetterling, W. T. 1986, Numerical Recipes (Cambridge ; Cambridge Univ. Press)

Rauch, T. 2000, A&A, 356, 665

Rauch, T. 2003, A&A, 403, 709

Rodríguez-López, C. et al. 2010, MNRAS, 402, 295

Rodríguez-López, C., Moya, A., Garrido R., MacDonald, J., Ulla, A., Dreizler, S., Hügelmeyer, S. D., Manteiga M., 2006, Balt. Astron., 15, 313

Werner, K. 1996, ApJ, 457, L39

Woudt, P. A. et al. 2006, MNRAS, 371, 1497

Chapitre 3

Conclusion

La détermination des paramètres atmosphériques des étoiles chaudes est un processus qui requiert des techniques de calculs sophistiquées et surtout, beaucoup de patience et de ressources, dû aux longs temps de calculs. La température élevée dans l'atmosphère de ces étoiles ne convient pas aux approximations de l'équilibre thermodynamique local et il faut alors utiliser les équations détaillées des conditions hors-ETL. Nos calculs de modèles d'atmosphères dans de telles conditions ont été effectués à l'aide du programme TLUSTY, initialement mis au point dans les années 80 par Ivan Hubeny et Thierry Lanz (Hubeny 1988) dans le but précis d'effectuer des calculs de modèles d'atmosphères hors-ETL d'étoiles chaudes. L'inclusion des métaux dans les modèles d'atmosphères est un deuxième élément important lorsqu'on veut déterminer les paramètres atmosphérique des sous-naines chaudes. Les métaux influencent de façon non-négligeable la structure en température de l'atmosphère de l'étoile, qui influence à son tour le spectre émergent, qui est utilisé pour faire les ajustements avec les spectres observés. En parallélisant TLUSTY, il nous est possible de calculer jusqu'à 80 modèles d'atmosphères à la fois, et c'est ainsi, en réduisant considérablement le temps total de calcul, que nous avons pu calculer des grilles complètes de modèles d'atmosphères et de spectres synthétiques d'étoiles sdO incluant des métaux.

Dans le cadre de ce projet nous avons calculé quatre grilles de modèles d'atmosphères hors-ETL incluant différentes compositions chimiques :

1. H et He ;

2. H, He et C, N, O en quantité solaire ;
3. H, He et C, N, O solaire avec Fe 1/10 solaire ;
4. H, He, et C, N, O, Fe en abondance solaire.

Puisque le but principal de la construction de ces grilles de modèles d'atmosphères est l'analyse de SDSS J1600+0748, nos grilles couvrent un intervalle de température centré autour de la température obtenue par Fontaine et al. (2008) ($\sim$ 70 000 K) soit de 60 000 K à 80 000 K par saut de 2 000 K. Nous couvrons aussi l'intervalle de gravité des étoiles sous-naines chaudes ($4.8 \lesssim \log g \lesssim 6.4$) par saut de 0.2 dex et avons inclus différentes abondances d'hélium comprises entre -4.0 $\lesssim \log N(\mathrm{He})/N(\mathrm{H}) \lesssim -0.0$ par saut de 0.5 dex.

En plus de l'étude de SDSS J1600+0748, nous avons analysé les effets des métaux sur différents aspects de nos modèles d'atmosphères.

La stratification en température de nos modèles est principalement influencée par le carbone, l'azote et l'oxygène. L'ajout du fer n'apporte que de légères modifications à la température des couches en surface. Toutefois, le réchauffement des couches plus profondes occasionné par l'ajout de fer est du même ordre que celui dû au C, N, O. Ces résultats viennent corroborer ceux de Dreizler & Werner (1993) et Haas et al. (1996) qui ont observé le même effet dans leurs modèles.

En comparant les profils des principales raies de Balmer et d'hélium obtenues avec nos différents modèles, on remarque que les raies Hα, Hβ, He II 4686 et He II 5412 sont les plus affectées par la présence de métaux. Il s'agit des raies qui se forment le plus haut dans l'atmosphère, là où la composition chimique influence de façon plus importante la structure en température. De plus, ces raies comportent une structure centrale en émission qui est particulièrement sensible à la présence de métaux. Tout comme pour la structure en température, l'ajout du fer ne modifie pas de façon considérable le profil des raies ; celui-ci est principalement déterminé par le C, N, O.

Pour connaître de façon globale les changements apportés par les métaux à nos spectres synthétiques, nous avons effectué des comparaisons entre nos différentes grilles. Des spectres de nos grilles avec métaux ont été considérés comme des spectres "observés" et nous avons effectué des ajustements de paramètres sur ces derniers en utilisant nos grilles de modèles

sans métaux. Mentionnons que l'abondance d'hélium est gardée fixe pendant ces procédures. Les différences entre les températures et gravités réelles de nos spectres et celles obtenues par la procédure d'ajustement nous permettent alors d'évaluer les effets globaux des métaux sur le spectre émergent (à tout le moins dans le domaine optique). Nous en concluons que ces effets dépendent à la fois de la température effective et de la gravité de surface ; l'ajout des métaux tend à augmenter la gravité de surface, alors que les différences en température ne sont pas systématiques. De plus, l'abondance d'hélium influence de façon importante les effets des métaux ; une faible abondance d'hélium ($\log N(\mathrm{He})/N(\mathrm{H}) \lesssim -1.5$) contribue à augmenter les effets des métaux (et par le fait même les différences entre les températures et gravités réelles et celles obtenues lors de l'ajustement) alors que ceux-ci seront moins prononcés lorsque l'abondance d'hélium est plus élevée.

Finalement, nous avons refait l'analyse spectroscopique du spectre de SDSS J1600+0748 obtenu au télescope de 2.3 m du Steward Observatory. Ce spectre a été initialement présenté par Fontaine et al. (2008), toutefois la procédure de réduction a été entièrement refaite pour la présente analyse (voir Annexe A). Notre meilleure ajustement est obtenu avec la partie "bleue" (3700 - 5600 Å) du spectre nettoyé et notre grille incluant C, N, O et Fe solaire, et mène aux paramètres suivants : $T_{\mathrm{eff}} = 68\ 500 \pm 1770$ K, $\log g = 6.09 \pm 0.07$, and $\log N(\mathrm{He})/N(\mathrm{H}) = -0.64 \pm 0.05$. Les paramètres atmosphériques obtenus avec nos différentes grilles hors-ETL ne diffèrent pas de façon significative entre eux, bien que, visuellement, on note une certaine amélioration de l'ajustement des profils de raies. Le fait est que SDSS J1600+0748, étant donné ses paramètres atmosphériques (particulièrement son abondance d'hélium), se trouve dans une région où les effets des métaux sont peu importants lorsque l'on considère le spectre visible. Ceci est facilement visible en regardant les cartes de la figure 2.7, où, pour des paramètres similaires à ceux de SDSS J1600+0748, le vecteur représentant les effets des métaux est très petit.

Dès que SDSS J1600+0748 sera observée dans le domaine ultraviolet, il sera possible d'effectuer une analyse détaillée des abondances métalliques de cette étoile. Il s'agira sans aucun doute d'un exercice intéressant, permettant de calculer ensuite un modèle d'atmosphère "personnalisé" pour SDSS J1600+0748 en y incluant les quantités appropriées de métaux.

Bibliographie

Baran, A., & Fox-Machado, L. 2009, Ap&SS, 285

Bergeron, P., Wesemael, F., Lamontagne, R., & Chayer, P. 1993, ApJ, 407, L85

Charpinet, S., Fontaine, G., Brassard, P., & Dorman, B. 1996, ApJ, 471, L103

Chavira, E. 1958, Boletin de los Observatorios Tonantzintla y Tacubaya, 2, 15

Chayer, P., Vennes, S., Pradhan, A. K., Thejll, P., Beauchamp, A., Fontaine, G., & Wesemael, F. 1996, IAU Colloq. 152 : Astrophysics in the Extreme Ultraviolet, 211

D'Cruz, N. L., Dorman, B., Rood, R. T., & O'Connell, R. W. 1996, ApJ, 466, 359

Dreizler, S., & Werner, K. 1993, A&A, 278, 199

Faulkner, J. 1972, ApJ, 173, 401

Feige, J. 1958, ApJ, 128, 267

Fontaine, G., Brassard, P., Green, E. M., Chayer, P., Charpinet, S., Andersen, M., & Portouw, J. 2008, A&A, 486, L39

Fontaine, G., Brassard, P., Charpinet, S., Green, E. M., Chayer, P., Randall, S., & Dorman, B. 2006, Proceedings of SOHO 18/GONG 2006/HELAS I, Beyond the spherical Sun, 624,

Gourgouliatos, K. N., & Jeffery, C. S. 2006, MNRAS, 371, 1381

Green, E. M., et al. 2003, ApJ, 583, L31

Green, E. M., Liebert, J. W., & Saffer, R. A. 1997, The Third Conference on Faint Blue Stars, 417

Gray, R.O., & Corbally, C.J. 2009, "Stellar Spectral Classification", (Princeton : Princeton University Press)

Han, Z., Podsiadlowski, P., Maxted, P. F. L., & Marsh, T. R. 2003, MNRAS, 341, 669

Han, Z., Podsiadlowski, P., Maxted, P. F. L., Marsh, T. R., & Ivanova, N. 2002, MNRAS, 336, 449

Haas, S., Dreizler, S., Heber, U., Jeffery, S., & Werner, K. 1996, A&A, 311, 669

Heber, U. 2009, ARA&A, 47, 211

Hirsch, H. A., Heber, U., & O'Toole, S. J. 2008, Hot Subdwarf Stars and Related Objects, 392, 131

Hubeny, I. 1988, Computer Physics Communications, 52, 103

Humason, M. L., & Zwicky, F. 1947, ApJ, 105, 85

Iriarte, B., & Chavira, E. 1957, Boletin de los Observatorios Tonantzintla y Tacubaya, 2, 3

Kilkenny, D., Koen, C., O'Donoghue, D., & Stobie, R. S. 1997, MNRAS, 285, 640

Koen, C., Kilkenny, D., O'Donoghue, D., van Wyk, F., & Stobie, R. S. 1997, MNRAS, 285, 645

Lanz, T., & Hubeny, I. 2007, ApJS, 169, 83

Lanz, T., Brown, T. M., Sweigart, A. V., Hubeny, I., & Landsman, W. B. 2004, ApJ, 602, 342

Lanz, T., & Hubeny, I. 2003, ApJS, 146, 417

Lanz, T., Hubeny, I., & Heap, S. R. 1997, ApJ, 485, 843

Lutz, R., et al. 2008, Hot Subdwarf Stars and Related Objects, 392, 339

Maxted, P. f. L., Heber, U., Marsh, T. R., & North, R. C. 2001, MNRAS, 326, 1391

Morales-Rueda, L., Maxted, P. F. L., Marsh, T. R., Kilkenny, D., & O'Donoghue, D. 2006, Baltic Astronomy, 15, 187

Napiwotzki, R. 2008, Hot Subdwarf Stars and Related Objects, 392, 139

Napiwotzki, R., Karl, C. A., Lisker, T., Heber, U., Christlieb, N., Reimers, D., Nelemans, G., & Homeier, D. 2004, Ap&SS, 291, 321

Napiwotzki, R. 1993, Acta Astronomica, 43, 343

O'Donoghue, D., Lynas-Gray, A. E., Kilkenny, D., Stobie, R. S., & Koen, C. 1997, MNRAS, 285, 657

Oreiro, R., Pérez Hernández, F., Ulla, A., Garrido, R., Østensen, R., & MacDonald, J. 2005, A&A, 438, 257

Østensen, R. H., et al. 2010, arXiv :1007.3170

Rauch, T. 2000, A&A, 356, 665

Rodríguez-López, C., Garrido, R., Moya, A., MacDonald, J., & Ulla, A. 2008, Hot Subdwarf Stars and Related Objects, 392, 363

Rodríguez-López, C., Ulla, A., & Garrido, R. 2007, MNRAS, 379, 1123

Saio, H., & Jeffery, C. S. 2000, MNRAS, 313, 671

Schuh, S., Huber, J., Dreizler, S., Heber, U., O'Toole, S. J., Green, E. M., & Fontaine, G. 2006, A&A, 445, L31

Söderhjelm, S. 1999, A&A, 341, 121

Stobie, R. S., Kawaler, S. D., Kilkenny, D., O'Donoghue, D., & Koen, C. 1997, MNRAS, 285, 651

Stroeer, A., Heber, U., Lisker, T., Napiwotzki, R., Dreizler, S., Christlieb, N., & Reimers, D. 2007, A&A, 462, 269

Sweigart, A. V. 1997, ApJ, 474, L23

Werner, K. 1996, ApJ, 457, L39

Werner, K. 1986, A&A, 161, 177

Woudt, P. A., et al. 2006, MNRAS, 371, 1497

Remerciements

Je tiens particulièrement à remercier mon superviseur Gilles, pour m'avoir déniché un projet que j'adore de plus en plus à mesure que j'en découvre de nouvelles facettes.

Ce projet n'aurait pas été possible sans l'aide de Pierre Brassard, notre inestimable "informaticien", et sans les connaissances de Pierre Chayer en matière de TLUSTY et SYNSPEC. Je dis aussi un gros merci aux filles du bureau, pour ensoleiller chacune de mes journées de travail. Merci à mes parents, pour toujours être fiers de moi et surtout pour m'avoir toujours encouragé à continuer mes études, même dans ce domaine "exotique".

Je voudrais finalement remercier aussi ma meilleure amie, et colocataire, pour son soutien quotidien et surtout pour, un jour, m'avoir accompagnée, par une froide soirée d'hiver, sur ma "butte" de neige pour regarder les étoiles. Sans cette soirée, peut-être bien que ce mémoire n'aurait jamais existé.

Annexe A

Inferring the Nature of the Companion Star

In order to identify as accurately as possible the secondary star in the J1600+0748 system, suitable main sequence (MS) template stars have been selected from lists of secondary spectral standards (see appendix A of Gray & Corbally 2009). They were observed multiple times during numerous observing runs using the same instrument and spectral setup as for J1600+0748. All of the spectra were reduced in the same homogeneous manner. The linearized spectra were computed with precisely the same starting wavelength and wavelength interval as were used for the target star (3625−6895 Å), and the individual spectra for each MS star were similarly velocity shifted and combined. Template spectra suitable for Fourier filtering and cross-correlation were obtained by dividing each combined spectrum by a smooth fit to its continuum and subtracting 1.0, in order to obtain a mean continuum level of zero.

The double-precision version of the IRAF task FXCOR was used to cross-correlate the combined continuum-removed spectrum of J1600+0748 with respect to the corresponding MS template spectra. A ramp filter was applied to the Fourier transforms of both the object and template spectra, using a standard set of filter parameters specific to our ccd and spectroscopic setup. The adopted parameters provide maximum cross-correlation sensitivity over the complete range of spectral types from O to M stars and from subdwarfs to giants. Specifically, the cuton and fullon parameters were chosen to limit the cross-correlation to features with FWHM

less than the width of typical Balmer lines in A stars and hot subdwarfs, while the adopted cutoff and fulloff parameters eliminated the contribution from features with FWHM smaller than the instrumental resolution. Finally, the cross-correlations of the J1600+0748 spectrum versus the MS templates were performed using the entire spectrum except that we excluded all wavelength intervals containing Balmer and He lines, to ensure that effectively all of the contributing spectral features came from the J1600+0748 secondary and not the sdO primary.

Table 2.5 summarizes the results of these cross-correlation exercises. The Tonry-Davis ratio (TDR) in column 1 is a measure of how well the image spectrum matches the template spectrum. The larger the ratio, the better the match. Alternately, one could consider the error in the differential velocities between the object and template spectrum (column 2), where a closer match between the spectral types results in a smaller $V_{\rm err}$. (Note that the velocity errors output by FXCOR are known only to within a multiplicative constant.) Using either the Tonry-Davis ratio or the velocity errors, it is clear that the combined spectrum of J1600+0748 matches best with the two stars of spectral type G0V, and that the correlation is worse for F8V, F9V, and G1V spectral types.

However, it also seems that there is an additional, although slightly poorer, correlation with stars whose spectral types are between G8V and K2V. The latter point is of considerable interest because it turns out that both of the G0V spectrum standards in our list, HD13974 = δ Tri and HD160269 = 26 Dra, turn out to be binary stars, and both have approximately 1.0 $M_{\odot}$ (early G) primaries and 0.7 $M_{\odot}$ (early K) secondaries. δ Tri is a nearly pole-on, double-lined binary with a period of about 10 d. Fuhrmann (2008) determined that the masses of δ Tri A and B are 0.99 and 0.74 $M_{\odot}$, respectively. The central binary of 26 Dra [1] has an orbital period of 76 years and a semi-major axis of 1.53″ (Söderhjelm 1999). The mass of the primary is estimated to be 1.08 $M_{\odot}$, with a secondary of 0.67 $M_{\odot}$.

In each case, the light from both the early G and the early K star would have been included in our 2.5″ spectroscopic slit. If the secondary in J1600+0748 is itself a G0V + early K binary, that would account for the strength of the cross-correlation peak with HD13974 and HD160269, as well as providing a natural explanation for the secondary peak near K0V.

1. 26 Dra also has a third M1Ve component about 12' distant.

TABLE A.1 – Results of our Cross-Correlation Procedure

TDR	$V_{\rm err}$ (km s^{-1})	Spectral Type	Template Object	S/N	Number of Spectra
12.12	26.50	F0V	HD110380	695.2	4
12.86	24.86	F2V	HD128167	740.0	6
10.98	29.43	F3V	HD26015	1063.5	12
11.22	29.36	F5V	HD27524	985.7	10
12.29	27.76	F8V	HD27808	973.9	10
11.70	29.10	F9V	HD27383	937.2	9
14.86	23.50	G0V	HD13974	1123.1	13
14.04	24.03	G0V	HD160269	733.0	9
11.45	30.18	G1IV	HD67228	1282.2	19
12.29	28.12	G1V	HD27836	1013.8	10
12.17	28.96	G2IV	HD217014	1026.6	10
11.14	30.99	G4V	HD117176	1164.4	16
12.28	28.93	G4V	HD214850	1051.2	12
13.30	25.88	G8V	GL566	1160.4	17
13.15	26.40	K0V	GL27	1360.3	24
11.84	28.50	K1IV	HD142091	1070.4	16
13.34	27.11	K1V	HD37008	459.5	3
11.71	28.67	K1V	HD90442	397.5	2
13.71	24.89	K2V	GL706	910.2	13
12.02	28.29	K2V	GL762.1	900.9	11
11.51	28.64	K2V	HD80492	430.3	2
10.59	31.97	K2V	HD290136	391.8	2
11.95	28.43	K3V	GL105A	1196.5	17
11.64	28.89	K4V	HD57901	1221.6	15
11.76	27.90	K5V	GL727	860.3	10
11.11	29.21	K5V	HD84035	350.0	2
10.24	31.22	K7V	GL820B	816.1	13
9.24	34.05	K7V	GL338B	1014.5	14
10.38	31.39	K7V	GL786	413.1	3
9.98	32.14	M0V	GL763	455.7	3
9.21	33.91	M0V	GL328	373.1	2
9.87	33.81	M0V	GL763	455.7	3

Because we do not have enough information to determine the exact spectral type(s) of the secondary, and also because the spectral features from early G to early K are rather similar, we decided to remove the MS contamination from the spectrum of the composite sdO star in a purely empirical manner. We averaged our two best-matching flux-calibrated G0V spectra, multiplied the result by a scaling factor and subtracted it from the combined flux-calibrated J1600+0748 spectrum. After removing the continuum from the subtracted spectrum, as before, it was once again cross-correlated against the averaged G0V template. The scaling factor was adjusted and the process repeated until the cross-correlation peak between the subtracted (decontaminated) sdO spectrum and the G0V template was minimized.